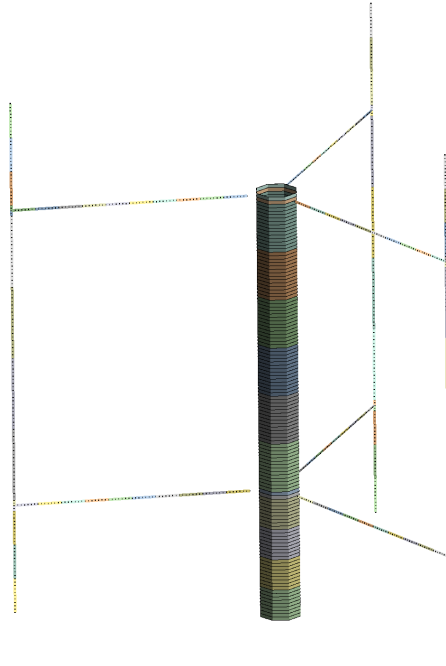




**CHALMERS**  
UNIVERSITY OF TECHNOLOGY



# Early Concept Evaluation of Floating Vertical Axis Wind Turbines

Method development and testing utilizing FE-modelling, structural optimization and H-rotor designs

Master's thesis in Product Development and Applied Mechanics

Karl Arvidsson  
Rebecka Bergström

**DEPARTMENT OF MECHANICS AND MARITIME SCIENCES**

---

CHALMERS UNIVERSITY OF TECHNOLOGY  
Gothenburg, Sweden 2022  
[www.chalmers.se](http://www.chalmers.se)



MASTER'S THESIS 2022:40

# Early Concept Evaluation of Floating Vertical Axis Wind Turbines

Method development and testing utilizing FE-modelling, structural  
optimization and H-rotor designs

Karl Arvidsson  
Rebecka Bergström



**CHALMERS**  
UNIVERSITY OF TECHNOLOGY

DEPARTMENT OF MECHANICS AND MARITIME SCIENCES  
CHALMERS UNIVERSITY OF TECHNOLOGY  
Gothenburg, Sweden 2022

Early Concept Evaluation of Floating Vertical Axis Wind Turbines  
Method development and testing utilizing FE-modelling, structural optimization  
and H-rotor designs  
Karl Arvidsson  
Rebecka Bergström

© Rebecka Bergström and Karl Arvidsson, 2022.

Supervisor: Mattias Haggärde Langqrie, Sigma Energy and Marine  
Examiner: Jim Brouzoulis, Department of Mechanics and Maritime sciences

Master's Thesis 2022:40  
DEPARTMENT OF MECHANICS AND MARITIME SCIENCES  
Chalmers University of Technology  
SE-412 96 Gothenburg  
Telephone +46 31 772 1000

Cover: Beam model constructed in Ansys, showing the rotor that was optimized.

Typeset in L<sup>A</sup>T<sub>E</sub>X  
Printed by Chalmers Reproservice  
Gothenburg, Sweden 2022

Early Concept Evaluation of Floating Vertical Axis Wind Turbines  
Method development and testing utilizing FE-modelling, structural optimization  
and H-rotor designs  
Rebecka Bergström and Karl Arvidsson  
Department of Mechanics and Maritime Sciences  
Chalmers University of Technology

## Abstract

This master thesis concerned constructing a method for evaluation of concepts of floating vertical axis wind turbines, FVAWT, with an H-rotor design at an early design phase. As optimization is used, further sub-concepts are also generated and evaluated. Furthermore, the method was utilized on two models for a 1 MW and 10 MW turbine. The project was conducted together with the company SeaTwirl. Their current turbine design was used to build the initial models. FE-modelling and optimization were performed in Ansys workbench. The focus was on structural modeling and optimization, with aerodynamic, gravitational, and centrifugal loads being the ones considered. The studied part of the FVAWT was the rotor, consisting of two struts per blade, three blades, and a tower. These parts were optimized with respect to cost by creating a goal function dependent on the mass and the vertical center of gravity. The considered structural constraints were the first eigenfrequency, fatigue of the tower, and the ultimate limit state, ULS, on blades and struts in form of maximum allowed strains. To facilitate the optimization, assumptions to simplify the model and reduce the number of parameters were introduced. The project resulted in a method considered feasible to obtain indications of an optimal design for a floating vertical axis wind turbine of H-rotor design. Possible designs for a 1 MW and a 10 MW rotor were also found by utilizing the developed method.



# Acknowledgements

This project had not been possible without the help and support of the people contributing from Chalmers, SeaTwirl and Sigma Energy and Marine. First we would like to thank our examiner Jim Brouzoulis at Chalmers for his support throughout the project. We would also like to thank our supervisor Mattias Haggärde Langqrie from Sigma Energy and Marine as well as Jonas Boström and Martin Rosander at SeaTwirl for their continuous contribution during this study. Finally we would like to thank everyone at Sigma Energy and Marine and SeaTwirl for providing equipment and expertise to make this project possible.

Karl Arvidsson, Gothenburg, June 2022

Rebecka Bergström, Gothenburg, June 2022





# List of Acronyms

Below is the list of acronyms that have been used throughout this thesis listed in alphabetical order:

AEP	Annual Energy Production
CAPEX	Capital Expenses and Expenditures
DOE	Design of experiment
FVAWT	Floating Vertical Axis Wind Turbine
HAWT	Horizontal Axis Wind Turbine
LCOE	Levelized cost of energy
MOGA	Multi-Objective Genetic Algorithm
OPEX	Operating Expenditures
S2X	SeaTwirl's current 1 MW FVAWT design
ULS	Ultimate Limit State
VCoG	Vertical Center of Gravity



# Nomenclature

Below is the nomenclature of terminology, indices, sets, parameters, and variables that have been used throughout this thesis.

## Terminology

FE Model	Rotor model with added quantities of load, force, mesh etc.
Optimization Model	The method used for optimizing the turbine model
Rotor	The upper part of the VAWT- tower, struts, blades etc.
Rotor Model	CAD models of the rotor with different complexities
VAWT	The full wind power plant with turbine, generator house etc.
NACA	Airfoil profile commonly used for wind turbine blades

## Parameters

$A$	Swept area
$A_{cs}$	Area of cross-section
$A_p$	Area of the blade perpendicular to $W$
$c$	Chord length
$C_d$	Drag coefficient
$C_l$	Lift coefficient
$CoG$	Centre of Gravity
$C_p$	Power coefficient, the ratio of available kinetic power in the wind and $P$
$D$	Total fatigue damage
$DFP$	Design fatigue factor
$\epsilon_{xx,N}$	strains induced by normal forces
$\epsilon_{xx,B}$	strains induced by normal forces

---

$F_t$	Tangential force
$I_{yy}$	Moment of inertia about the Y axis
$I_{zz}$	Moment of inertia about the Z axis
$J$	Torsional constant
$K$	Weight for cost function
$\kappa$	The curvature of the cross section
$\lambda = v/V$	Tip speed ratio
$L_{\text{blade}}$	Blade length
$M$	Bending moment
$m_{\text{blade}}$	Mass blade
$m_{\text{strut}}$	Mass struts
$m_{\text{tower}}$	Mass tower
$N$	Number of blades
$\omega$	Angular velocity of rotor
$P$	Generated output power
$\phi$	The rotation of the cross section
$\rho_{\text{air}}$	Air density
$R_o$	Outer radius tower
$R_i$	Inner radius tower
$s$	Solidity
$\sigma$	Stress amplitude
$V$	Free wind speed
$v$	Rotor tip speed
$VCoG$	Vertical Centre of Gravity
$W$	Relative velocity between the wind and the blade

## Design Variables

$AP_{\text{strut},i,p}$	Design variable for tower-strut attachment points
$CS_{\text{strut}}$	Design variable for cross section properties of the strut
$CS_{\text{Blade}}$	Design variable for cross section properties of the blade
$I_{\text{strut},i,p}$	Design variable for strut inclination
$R$	rotor radius

# Contents

<b>List of Acronyms</b>	<b>ix</b>
<b>Nomenclature</b>	<b>xi</b>
<b>List of Figures</b>	<b>xv</b>
<b>List of Tables</b>	<b>xvii</b>
<b>1 Introduction</b>	<b>1</b>
1.1 Background . . . . .	1
1.1.1 Vertical axis offshore wind power . . . . .	2
1.1.2 Early Stage Product Development . . . . .	3
1.1.3 SeaTwirl . . . . .	5
1.2 Aim . . . . .	6
1.3 Limitations . . . . .	7
1.4 Report outline . . . . .	8
<b>2 Theory</b>	<b>9</b>
2.1 Wind power turbines . . . . .	9
2.1.1 Technical aspects of FVAWT . . . . .	9
2.1.2 FVAWT loads . . . . .	11
2.2 Structural modeling . . . . .	13
2.3 Optimization . . . . .	15
2.3.1 General optimization theory . . . . .	15
2.3.2 Optimization tools in Ansys . . . . .	17
2.4 Cost analysis . . . . .	18
2.4.1 LCOE . . . . .	18
2.4.2 FVAWT costs . . . . .	19
<b>3 Methodology</b>	<b>21</b>
<b>4 Optimization method</b>	<b>23</b>
<b>5 H-rotor setup</b>	<b>27</b>
5.1 Prerequisites . . . . .	27
5.1.1 The concept of a VAWT with H-rotor . . . . .	27
5.1.2 Load analysis . . . . .	28

5.1.3	Tools used in the optimization . . . . .	28
5.2	Goal function . . . . .	29
5.3	Constraints . . . . .	30
5.3.1	Eigenfrequency . . . . .	31
5.3.2	Strain . . . . .	31
5.3.3	Fatigue . . . . .	31
5.4	Parameters and design variables . . . . .	32
5.4.1	Strut . . . . .	32
5.4.2	Blade . . . . .	33
5.4.3	Tower . . . . .	34
5.4.4	Further parameters . . . . .	34
5.5	Modelling . . . . .	35
5.5.1	Cross-section properties . . . . .	35
5.5.2	Loads and boundary conditions . . . . .	37
5.5.3	Coordinate systems . . . . .	38
5.5.4	Struts . . . . .	40
5.5.5	Blades . . . . .	40
5.5.6	Tower . . . . .	40
5.5.7	Connections . . . . .	41
5.5.8	Additional mass . . . . .	41
5.5.9	Mesh . . . . .	42
5.6	Optimization flow . . . . .	43
<b>6</b>	<b>H-rotor designs</b>	<b>47</b>
6.1	Initial designs . . . . .	47
6.1.1	1 MW . . . . .	48
6.1.2	10 MW . . . . .	49
6.2	Optimized designs . . . . .	50
6.2.1	1 MW . . . . .	50
6.2.2	10 MW . . . . .	53
<b>7</b>	<b>Discussion</b>	<b>57</b>
7.1	Method development . . . . .	57
7.2	Optimization results . . . . .	58
<b>8</b>	<b>Conclusion</b>	<b>61</b>
<b>9</b>	<b>Future work</b>	<b>63</b>
<b>A</b>	<b>Appendix A</b>	<b>I</b>
<b>B</b>	<b>Appendix B</b>	<b>V</b>
B.1	1 MW inputs . . . . .	V
B.2	10 MW inputs . . . . .	VII

# List of Figures

1.1	Example of a horizontal axis wind turbine, HAWT, to the left and a vertical axis wind turbine, VAWT, to the right [6] . . . . .	2
1.2	Outline of the steps in the Ulrich & Eppinger development process [13].	3
1.3	Example of the development funnel described by Wheelwright & Clark [14]. . . . .	5
1.4	Breakdown of the parts of Seatwirl's current FVAWT design, the S2X, generating up to 10 MW [15]. . . . .	5
2.1	Example of the geometry of a straight bladed vertical axis wind turbine.	9
2.2	The geometry of a NACA airfoil - 1: Leading edge, 2: Maximum thickness, 3: Camber, 4: Camber mean line, 5: Chord line, 6: Trailing edge. . . . .	10
2.3	A three bladed VAWT seen from above with its tip speed, $v$ , the wind speed, $V$ , and relative velocity, $W$ (left). The force and its different components acting on a blade profile (right). . . . .	12
2.4	Geometry of a BEAM188 element, figure from Ansys help [24]. . . . .	13
2.5	Outline of the DesignXplorer's parametric optimization tools. The orange arrows indicates where connections can be created manually [24]. . . . .	17
2.6	Outline of the cost for a FVAWT as described by Sandia National Laboratories [8]. . . . .	19
4.1	Description of the full evaluation method developed for H-rotor designs.	23
5.1	Breakdown of the parts of Seatwirl's current FVAWT design, the S2X [15]. . . . .	27
5.2	Global model from the Principia analysis. . . . .	28
5.3	The black points marks the places at which the strains were calculate for the blades and the struts. . . . .	31
5.4	The design variables affecting the geometry of the rotor. The black dots are located at the initial positions and the arrows show how the dots can vary depending on the values of the design variables. . . . .	33
5.5	Average, maximum, and minimum tangential force for different wind speeds. . . . .	37
5.6	Loads applied on the FE model. A, B, and C represents the aerodynamic loads, E represents the centrifugal force, F represents the gravitational force and D shows the fixed boundary condition. . . . .	38

5.7	Coordinate systems for cross-sections in Design Modeler and Ansys, figure taken from Ansys Help [24]. . . . .	38
5.8	Local coordinate systems in which the aerodynamic forces are applied. . . . .	39
5.9	The global coordinate system having its origin at the bottom of the spar buoy (not shown). . . . .	39
5.10	One strut divided in sections (colour scheme) and elements (dots). . . . .	40
5.11	One blade divided in sections (colour scheme) and elements (dots). . . . .	40
5.12	The tower divided in sections (colour scheme) and elements (lines). . . . .	41
5.13	Illustration of a connection between the tower and one of the struts. . . . .	41
5.14	Outline of the DesignXplorer parametric optimization tools [24]. Only direct optimization was used out of all methods tried, as illustrated by the red circle. . . . .	43
6.1	The initial design of the rotor, isometric view. . . . .	47
6.2	The initial design of the turbine, blade view. . . . .	47
6.3	Candidate point 1 from optimization 1 MW fixed, design 1 and design 2. . . . .	50
6.4	Candidate point 1 from optimization 1 MW pinned, design 1 and design 2. . . . .	52
6.5	Candidate point 1 from optimization 10 MW fixed, design 1. . . . .	53
6.6	Candidate point 1 from optimization 10 MW fixed, design 2. . . . .	53
6.7	Candidate point 1 from optimization 10 MW pinned, design 1. . . . .	55
6.8	Candidate point 1 from optimization 10 MW pinned, design 2. . . . .	55
A.1	Candidate point 2 from optimization 1 MW fixed, design 1. . . . .	I
A.2	Candidate point 3 from optimization 1 MW fixed, design 1. . . . .	I
A.3	Candidate point 2 from optimization 1 MW pinned, design 1. . . . .	I
A.4	Candidate point 3 from optimization 1 MW pinned, design 1. . . . .	I
A.5	Candidate point 2 from optimization 10 MW fixed, design 1. . . . .	II
A.6	Candidate point 3 from optimization 10 MW fixed, design 1. . . . .	II
A.7	Candidate point 2 from optimization 10 MW fixed, design 2. . . . .	II
A.8	Candidate point 3 from optimization 10 MW fixed, design 2. . . . .	II
A.9	Candidate point 2 from optimization 10 MW pinned, design 1. . . . .	II
A.10	Candidate point 3 from optimization 10 MW pinned, design 1. . . . .	II
A.11	Candidate point 2 from optimization 10 MW pinned, design 2. . . . .	III
A.12	Candidate point 3 from optimization 10 MW pinned, design 2. . . . .	III



# List of Tables

4.1	Outline of the constructed method for evaluation of H-rotors. . . . .	24
6.1	Design variables used in the first 1 MW optimizations. . . . .	48
6.2	Design variables used in the 10 MW optimizations. . . . .	49
6.3	Design variables, constraints, and the goal function for candidate points from optimization 1 MW fixed, design 1. . . . .	51
6.4	Design variables, constraints, and the goal function for candidate points from optimization 1 MW fixed, design 2. . . . .	51
6.5	Old and updated design variables, constraints, and the goal function for 1 MW fixed, design 3. . . . .	51
6.6	Design variables, constraints, and the goal function for candidate points from optimization 1 MW pinned, design 1. . . . .	52
6.7	Design variables, constraints, and the goal function for candidate points from optimization 1 MW pinned, design 2. . . . .	53
6.8	Old and updated design variables, constraints, and the goal function for 1 MW pinned, design 3. . . . .	53
6.9	Design variables, constraints, and the goal function for candidate points from optimization 10 MW fixed, design 1. . . . .	54
6.10	Design variables, constraints, and the goal function for candidate points from optimization 10 MW fixed, design 2. . . . .	54
6.11	Design variables, constraints, and the goal function for candidate points from optimization 10 MW pinned, design 1. . . . .	55
6.12	Design variables, constraints, and the goal function for candidate points from optimization 10 MW pinned, design 2. . . . .	55
B.1	Inputs for the cost analysis for the 1 and 10 MW cost weight analysis.	V
B.2	The inputs for the thrust moment calculations for the 1 MW rotors. .	V
B.3	The inputs and results for the S-N curve calculations for the 1 MW models. . . . .	VI
B.4	The factors used to scale the forces from the Principia report. . . . .	VI
B.5	Fixed parameters for the 1 MW rotors. . . . .	VI
B.6	Parameters governed by design variables for the 1 MW and 10 MW optimization, index $j$ stands for strut 1 or 2. . . . .	VII
B.7	The inputs for the thrust moment calculations for the 10 MW rotors.	VII
B.8	The inputs and results for the S-N curve calculations for the 10 MW models. . . . .	VIII
B.9	Fixed parameters for the 10 MW rotors. . . . .	VIII



# 1

## Introduction

In this section, some initial information about wind energy is introduced together with a presentation of SeaTwirl and their product. Furthermore, the aim and limitations of this project are stated as well as an outline of the full report.

### 1.1 Background

As the threat of climate change becomes increasingly relevant and urgent, the need for new, sustainable technologies to counter it has become more apparent. Renewable energy sources are a vital part of the transition towards a more climate-sustainable world, with wind energy being a major player in this field. The global wind industry had a year-on-year increase of about 53 percent in 2020. This trend is expected to continue with more wind power being installed every year, especially as this growth is still not sufficient to stay on a net-zero pathway [1]. According to the International Energy Agency 2021 forecast, the global wind power market is predicted to reach between 100-140 GW annual additions in 2026 [2], compared to the 743 GW installed today [1]. Only solar photovoltaic cells are forecasted to have a larger increase and contribute more to the renewable energy sector between these years [2].

As wind energy grows, new technologies and areas within the field are expected to emerge. Most noticeably, the market is predicted to move towards offshore wind turbines [3]. While onshore wind power is still predicted to stand for most of the energy by 2026, offshore is showing great potential and is expected to reach almost 120GW in 2026. Offshore is also expected to grow more rapidly than onshore wind power annually [2]. Furthermore, a newfound interest in vertical axis wind turbines has emerged and development in this area is expected to increase in the coming years [3].

With new technologies emerging, and ambitious goals such as the net zero pathway set, there is a strong need for efficient product development in the energy sector. Not only does offshore wind brings new challenges, but also technologies such as vertical axis wind turbines need massive improvement.

### 1.1.1 Vertical axis offshore wind power

As the market expands, finding suitable placements for wind turbines on land have become increasingly difficult. Therefore, alternative placements has become necessary to reach the goals for renewable energy and wind energy expansion. Subsequently, the development of wind turbines for offshore placements has taken off during the last few decades [4]. Historically, this type of wind power has not been relevant as it faces issues with higher complexity compared to traditional, land-based wind power turbines, mainly due to the changing environment at sea [5]. Structures at sea must be developed to withstand far more difficult weather conditions, such as unreliable winds and high waves, while also being relatively easy to maintain. Furthermore, the electrical networks connecting the offshore wind farms to the consumer centers might be long, and therefore costly and complex. Still, there are some clear advantages to offshore wind power. While the amount and freedom of placement compared to land-based wind turbines is a major benefit, the accessible wind quality is also better, with higher and more uniform wind speeds. The offshore wind turbines could therefore possibly generate much more electricity [5].

Offshore wind comes with new challenges. It is therefore highly relevant to reevaluate the way wind turbines are designed and produced today, as the traditional types of wind turbines might not be the most suitable for this placement. Wind turbines can be classified in different ways, but are primarily sorted according to the relative position of the rotor shaft to the ground and the type of forces on the blades. In the first classification way, wind turbines can be categorized into horizontal axis wind turbines, HAWTs, or vertical axis wind turbines, VAWTs, which are shown in Figure 1.1. In the second way, the main turbine types are called lift-type wind turbines and drag-type wind turbines [7]. In this project, the focus is on VAWTs and lift-type turbines. Over the years, VAWTs have been researched to a lower extent compared to HAWTs. VAWTs have overall been less attractive on the market, due to a variety of reasons such as efficiency and production price. However, recent developments in the wind energy sector have resulted in a newfound interest in this technology [7].

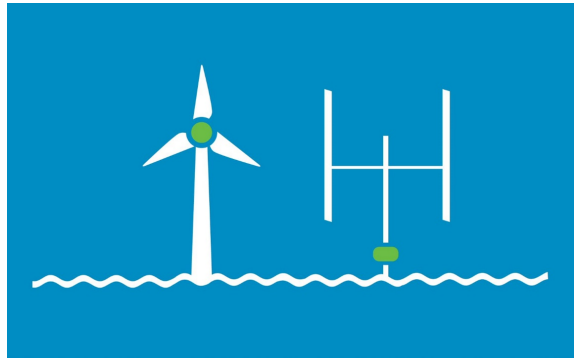


**Figure 1.1:** Example of a horizontal axis wind turbine, HAWT, to the left and a vertical axis wind turbine, VAWT, to the right [6]

The first reason for the increased interest in VAWTs is that the HAWT technology might have started to reach a plateau where it is difficult to further develop the concept and scale up the wind turbines [8]. The power output generated by a wind turbine is directly related to the swept area of its blades, and a horizontal axis wind turbine is expected to need a rotor diameter of up to 250 m to be able to generate 20 MW. This has a severe effect on the loads, weights, and other conditions of the wind

turbine, resulting in that HAWTs must rely on future breakthrough technology to reach these megawatt outputs [9].

Furthermore, there are some problems concerning the use of HAWTs in large-scale wind farms. Wind turbines cause a wake effect, meaning that the wind behind the turbine has a lower wind speed and increased turbulence. In a large-scale wind farm, this causes lower efficiency and potentially larger aerodynamical loads on downwind turbines [10]. This might result in a decrease of efficiency by up to 40% of downstream turbines depending on the wind conditions. Instead, VAWTs seem to exhibit the opposite behaviour and might even enhance each other's performance in a large-scale wind farm by up to 15%. An increasing number of turbines in a farm has also been shown to increase the overall capacity [11].

Finally, Offshore turbines can both be placed on the ocean-floor and be floating. This project will consider a floating axis wind power turbine, FVAWT. VAWTs have the advantage that all of the heavy equipment associated with power generation can be placed below the rotor. This leads to a lower center of gravity, which is important to increase stability for a floating structure, as well as considerably simplifying maintenance due to more accessible service points. VAWTs can also operate with winds from all directions without a yaw system, which may lead to a large reduction in cost for multi-megawatt turbines as these systems are a major expense for a HAWT system [12].

### 1.1.2 Early Stage Product Development

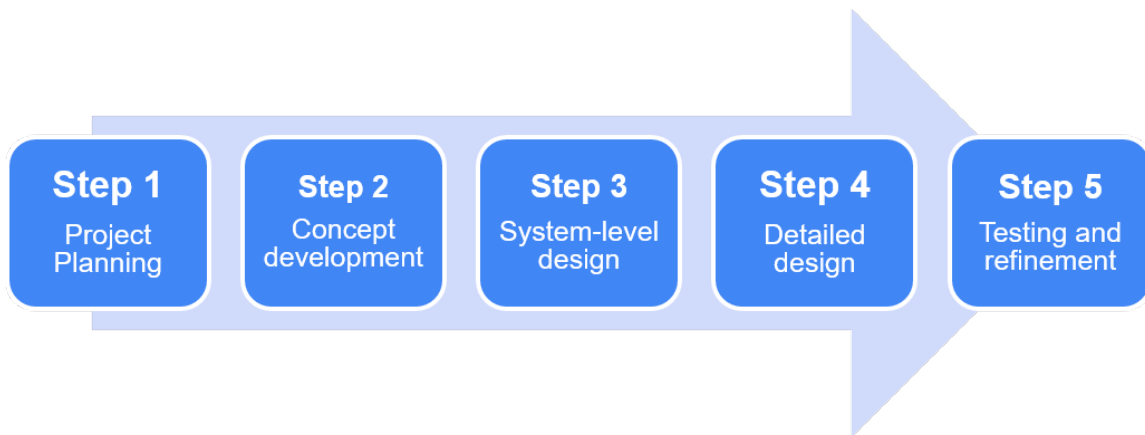


**Figure 1.2:** Outline of the steps in the Ulrich & Eppinger development process [13].

As mentioned in Section 1.1.1, VAWT technology is far from reaching the level of maturity of HAWT technologies. There is a variation of different possible designs, such as a Darrius rotor, a V-rotor, and an H-rotor, with no clear consensus on which design that is most effective [12]. Furthermore, offshore wind energy is still a relatively novel field, especially considering floating offshore structures. Therefore, there is a need for efficient product development for floating offshore structures and

VAWTs to be able to compete with the more developed areas of onshore structures and HAWTs.

A full product development process can be described in the five steps defined by Ulrich & Eppinger [13] seen in Figure 1.2. In this thesis, the focus will be on step 2, Concept development. This is often regarded as the design phase and can be divided into functional description, concept generation, and concept evaluation. The functional description outlines the inputs and outputs of the system and the functionality of each system part. The concept generation phase should be executed in iterations and with a multitude of different approaches. As many variations and concepts of the product as possible should be found. Finally, these concepts should be evaluated to find which concepts, or concept, that should continue to the next stage of more in-depth development. To evaluate concepts, a variety of methods ranging from using intuition to more thorough tools such as decision matrices can be used. For fair evaluation, however, it is important to use a structured method to ensure that the best concept is found and not the one that initially seems the most promising [13].

The concept development phase should be done in iterative and with increasingly complex designs. The phase typically starts with a broad range of inputs, which are then gradually narrowed down through rounds of evaluation and comparison. This indicates that after a first evaluation has been done, functional description and concept generation should once again be considered with the new knowledge found during the process. For example, concepts remaining from the first round might be combined and create a new set of concepts for evaluation. Furthermore, evaluation with a set of different tools might be conducted on the same set of concepts as one tool might not adequately compare all concepts. In the book *Revolutionizing product development* [14] the iteration of generation and evaluation is described through a development funnel, see Figure 1.3, where a large number of initial ideas gradually go through screenings as more information is found. In the end, one or a handful of ideas that can be turned into formal projects remain. The difficulties regarding this funnel, and the concept development phase, are to ensure a wide opening, whereas many ideas as possible are considered, and then efficiently narrow the funnel while ensuring that the right ideas last until the end. Not eliminating concepts too quickly while also narrowing the funnel is essential for correct and efficient product development [14].

Conducting correct and efficient product development in the concept development step is a great challenge when novel products, such as a FVAWT, are concerned. There are a large number of possible concepts to evaluate while there might not be enough knowledge or tools to make correct evaluations. For example, using a decision matrix where concepts are ranked against each other, might not be possible when very little knowledge exists regarding each concept. To tackle these problems regarding FVAWT, it is of interest to find a method to quickly obtain information regarding concepts with which they can then be compared.

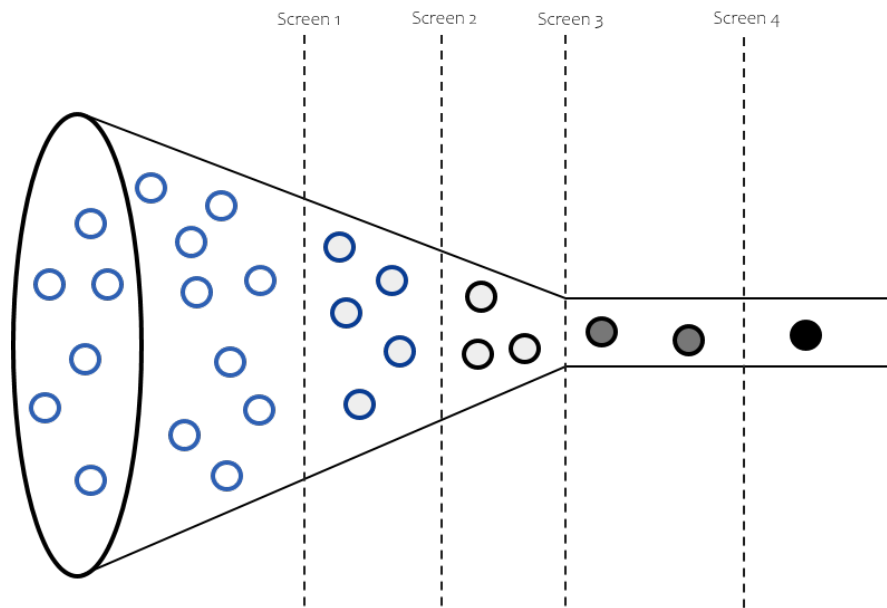


**Figure 1.3:** Example of the development funnel described by Wheelwright & Clark [14].

### 1.1.3 SeaTwirl

SeaTwirl was founded in 2012 in Gothenburg, based on the invention of a new concept for off-shore wind power by Daniel Ehrnberg. In 2015, SeaTwirl placed their first prototype, the S1, in the ocean outside the city Lysekil in Sweden. The S1 can generate up to 30kW and has been supplying the grid with electricity according to plan over the years. SeaTwirl plans on releasing their first commercial product, the S2X, in 2022. The S2X can generate up to 1 MW and the goal is to sell it to large offshore wind power farm projects. The company will then shift development focus towards larger turbines with an aim to be market-leading in the offshore industry by 2030 [15]. The S2X rotor design can be seen in Figure 1.4. Some key benefits of the SeaTwirl concept are linked to the advantages of VAWTs discussed in Section 1.1.1, but there are also further competitive advantages. Compared to other similar concepts of VAWT, the structure is of relatively low cost and easy to maintain [15].



**Figure 1.4:** Breakdown of the parts of Seatwirl's current FVAWT design, the S2X, generating up to 10 MW [15].

### 1.2 Aim

The aim of the project is divided into two parts:

1. Construct a method for efficient evaluation of the rotor part of an H-rotor VAWT at an early stage of product development.
2. Utilize this method on a 1 MW and 10 MW H-rotor to find indications regarding the optimal design.

The method will consist of FE-modelling and optimization, and have the ability to evaluate numerous concepts as a tool in the concept evaluation step described in Section 1.1.2. The method should be adapted for FVAWT at an early stage of development. This method is then tested with the aim to analyse and obtain reliable results regarding the optimal H-rotor design at two different power outputs. The optimal design in this project is the least costly rotor that still fulfills the defined constraints. The initial designs are based on the SeaTwirl S2X. While the method should preferably be utilized to narrow down several concepts, it is within the scope of this thesis only tested on an H-rotor with a few variations.



## 1.3 Limitations

The scope of this project is limited to:

- Aerodynamic, gravitational and centrifugal loads, which are implemented in static analyses.
- Optimization of the rotor with respect to cost, including the blades, the struts, and the tower.
- Design criteria containing constraints on eigenfrequency, maximum strain in the struts and the blades, and fatigue life of the tower.
- Aerodynamic performance, based on previous analysis, assumed to be constant during optimization.
- Cost analysis focused only on material cost.
- The concept of SeaTwirl's S2X, i.e. a H-rotor with three blades and two struts per blade.
- Only the materials used in SeaTwirls current design are considered, which are steel in the tower and composite material in the struts and blades.
- The use of Ansys Workbench and the optimization methods and algorithms available in DesignExplorer (part of the Ansys suite).

Due to the complexity of the real structure, a lot of simplifications and assumptions have to be made throughout the project, which will further limit the project scope. To figure out these limitations will be a big part of the work moving forward and will be further discussed in Section 5.

### 1.4 Report outline

This report begins with introducing the project through a short background about FVAWT, SeaTwirl, the renewable energy market and the product development process in Section 1. Thereafter, the aim and limitation has been defined in the same section. In Section 2, overall background theory regarding the important steps of the project; the development process, FE-modelling and optimization, is outlined. The theory are divided into five sections: product development, wind power turbines, structural modelling, optimization and cost analysis. Furthermore, specific theory for the tool of choice, ANSYS Workbench, is described.

In Section 3, the approach to carrying out the project is described, before the developed optimization method, connected to the first aim, can be found in Section 4. Section 5 outlines how the method has been used to reach a result regarding the optimal H-rotor design for the 1 MW and 10 MW rotor before Section 6 presents the final inputs and results connected to the second point of the aim. The results and findings from Section 5-6 are further discussed in Section 7 before the conclusion of the full project is presented in Section 8. Finally, future possible works and recommendations are presented in Section 9.

# 2

## Theory

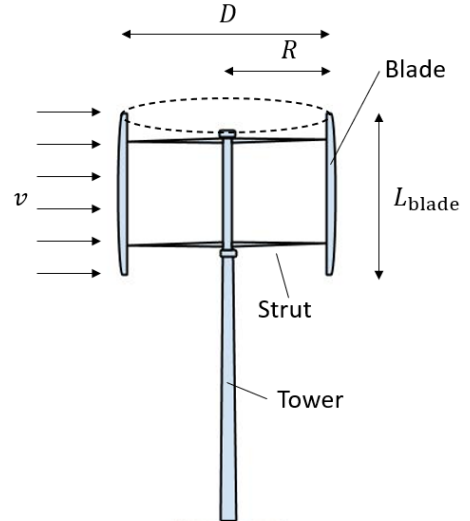
In this chapter, the theory relevant to this project is presented. General information regarding FE modeling and optimization is described to set the base for the following chapters.

### 2.1 Wind power turbines

In this Section, theory about wind turbines that are relevant for the assumptions made and the building of the FE model is stated. This includes for example the geometry, the efficiency, and the loads affecting wind turbines.

#### 2.1.1 Technical aspects of FVAWT

An example of the geometry and the parts of a straight bladed vertical axis wind turbine, SB-VAWT, is shown in Figure 2.1. The swept area of a SB-VAWT is defined as the diameter of the turbine times the blade length, i.e.  $A = D_{\text{turbine}} L_{\text{blade}} = 2RL_{\text{blade}}$ . The relation between  $D_{\text{turbine}}$  and  $L_{\text{blade}}$  is called the rotor aspect ratio and defined as  $L_{\text{blade}}/D_{\text{turbine}}$ . In a study of Ahmadi-Baloutaki et al. [16], a 3-bladed SB-VAWT with NACA0015 profiles, later described in this section, was studied. The result showed that the optimal rotor aspect ratio from an aerodynamic point of view lies between 0.5 and 2 with the best performance at  $L_{\text{blade}}/D_{\text{turbine}} = 1$  [16].



The number of struts per blade and the location of the struts are important parameters when it comes to the structural analysis of a VAWT. Ahmadi-Baloutaki et al. and Hameed et al. have shown that two struts with optimal locations of the strut to blade connections at 21% and 79% of the blade length will minimize the bending stresses in the blades [16, 17].

**Figure 2.1:** Example of the geometry of a straight bladed vertical axis wind turbine.

One of the most used profiles for wind turbine blades is the airfoil type called the NACA 4-digit series. The geometry of a NACA airfoil is shown in Figure 2.2. The leading edge is the point at the front of the airfoil while the trailing edge is the rear point of the airfoil. A straight line from the leading edge to the trailing edge is called the chord line and the length of it, the chord  $c$ , is an important dimension of an airfoil. The relation between the thickness and the chord is defined by the two last digits in the NACA 4-digit name, as they define the maximum thickness of the chord in percentage. The first two digits describe the possible asymmetry of the airfoil, defined as the camber and the position of the maximum camber [18].

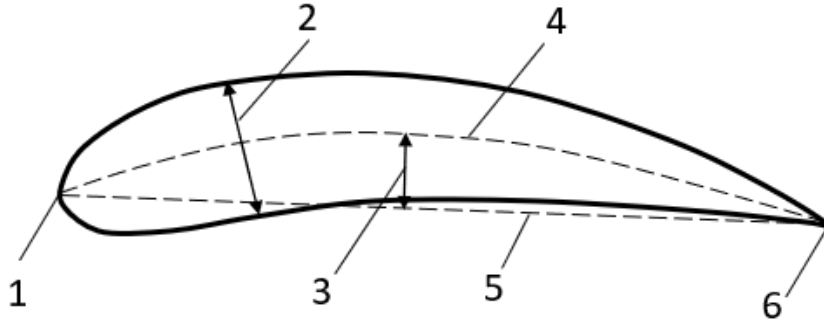


**Figure 2.2:** The geometry of a NACA airfoil - 1: Leading edge, 2: Maximum thickness, 3: Camber, 4: Camber mean line, 5: Chord line, 6: Trailing edge.

The solidity,  $s^1$ , of a VAWT is the total area of the blades divided with the swept area:

$$s = \frac{Nc}{2R} \quad (2.1)$$

where  $N$  is the number of blades [19]. The optimal solidity  $s_{\text{opt}}$  is different for different VAWTs. Multiple studies have shown that  $s_{\text{opt}}$  lies in the range 0.2 to 0.6 [16].

When it comes to the generated output power,  $P$ , from a wind turbine, it can be estimated as:

$$P = \frac{1}{2} \rho_{\text{air}} V^3 A C_p \quad (2.2)$$

where  $\rho_{\text{air}}$  is the air density,  $V$  is the free wind speed, and  $C_p$  is the power coefficient [20]. The power coefficient  $C_p$  is the ratio of the  $P$  and the available kinetic power in the wind and is a measure of the efficiency of the wind turbine [21]. It can be

---

<sup>1</sup>Solidity is often abbreviated as  $\sigma$ . However, to avoid confusion with stress, solidity is abbreviated as  $s$  in this report.

shown that the theoretical maximum value of  $C_p$  is 0.59, which is called the Betz Criterion. In reality,  $C_p$  is in general between 0.40 and 0.50 for a HAWT. Even if there is a lack of  $C_p$  values for VAWTs, a general opinion is that VAWTs have lower  $C_p$  compared to HAWT. However, studies have shown that the theoretical maximum  $C_p$  for VAWT might be larger than earlier assumed, even leading to questions if the Betz Criterion is the limit for VAWTs'  $C_p$  value [20]. From Equation (2.2), it can be noted that a turbine with a different rotor aspect ratio,  $L_{\text{blade}}/D_{\text{turbine}}$ , but with the same swept area, will generate the same output power. However, the rotor aspect ratio will in reality affect both the structural and aerodynamic performance,  $C_p$ , of a VAWT.

$C_p$  is dependent on another important parameter of wind turbines, the tip speed ratio,  $\lambda$ , defined as:

$$\lambda = \frac{v}{V} = \frac{\omega R}{V} \quad (2.3)$$

where  $v$  is the rotor tip speed and  $\omega$  is the angular velocity of the rotor. If  $\lambda$  is too small, too much wind passes the blades without any energy extraction. On the other hand, a too-large  $\lambda$  will create plenty of drag and consequently increase the losses. Hence, it is important to operate close to the optimal value,  $\lambda_{\text{opt}}$ , which differs among wind turbine designs [22].

Furthermore, the optimal relation between  $\lambda$  and  $s$  has been studied. Since the power output  $P$  is a function of  $A$  and  $V$  as  $P = P(AV^3)$ , the dimensionless power coefficient,  $C_p$ , can be considered to be a function of the corresponding dimensionless parameters  $s$  and  $\lambda$  in form of  $C_p = C_p(s\lambda^3)$ . Numerical analyses have confirmed this and that the relation between  $C_p$  and  $s\lambda^3$  is almost constant for different number of blades and solidity [19].

The frequency of the rotor revolution of a wind turbine is called the 1P frequency. The 3P frequency of a three-bladed turbine is three times larger than the 1P frequency of the same turbine and is the frequency of a blade passing the tower. To avoid increased dynamic loads and resonance, it must be verified that the wind turbine does not operate such that the 1P and 3P frequencies, for three-bladed turbines, are within  $\pm 10\%$  from the first natural frequency of the turbine [21].

### 2.1.2 FVAWT loads

The aerodynamic loads on the blades induce lift and drag, which can be decomposed into tangential and normal forces. The aerodynamic forces and the velocity components are shown in Figure 2.3.

The acting forces will vary during one revolution due to the variation in wind velocity and the angle of attack,  $\alpha$ . To determine the output power in one revolution, the instant tangential force on each blade,  $F_t$ , is first integrated to derive the average

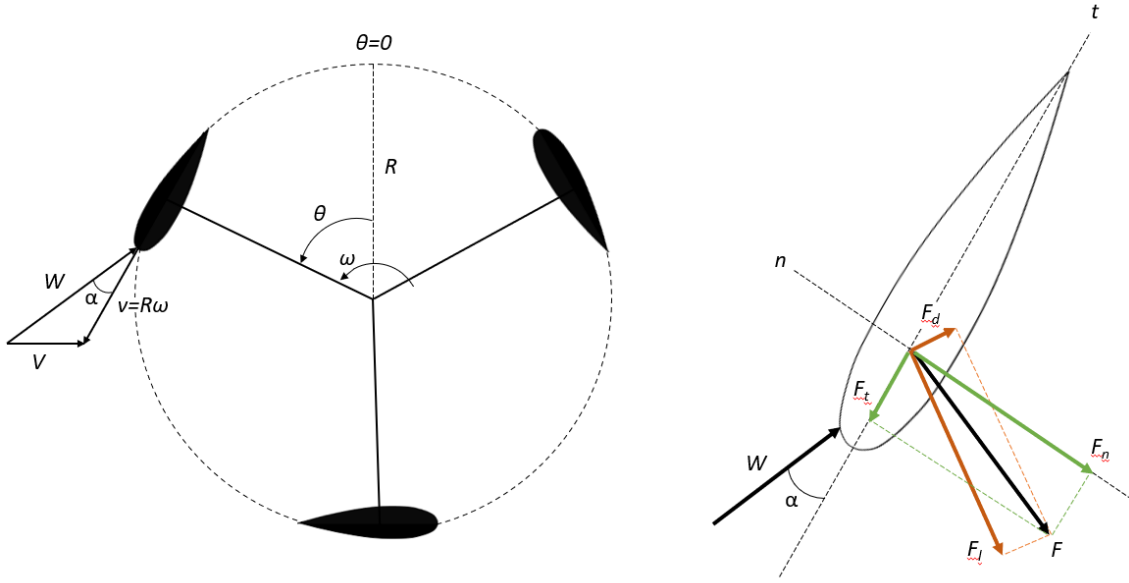


**Figure 2.3:** A three bladed VAWT seen from above with its tip speed,  $v$ , the wind speed,  $V$ , and relative velocity,  $W$  (left). The force and its different components acting on a blade profile (right).

tangential force,  $\bar{F}_t$  [16]:

$$\bar{F}_t = \frac{1}{2\pi} \int_0^{2\pi} F_t(\theta) d\theta \quad (2.4)$$

where  $\theta$  is the azimuthal angle. Furthermore, the dynamic torque about the tower axis,  $T$ , is determined by  $\bar{F}_t$  times the the rotor radius,  $R$ , and the number of blades  $N$ , implying following expression for the output power [16]:

$$P = T\omega = N\bar{F}_t\omega R \quad (2.5)$$

The instant tangetial force,  $F_t$ , and the instant normal force,  $F_n$ , on the blades are estimated by [16]:

$$F_t = \frac{1}{2} C_t \rho_{\text{air}} A_p W^2 \quad (2.6)$$

$$F_n = \frac{1}{2} C_n \rho_{\text{air}} A_p W^2 \quad (2.7)$$

where  $W$  is the relative velocity between the blade and the wind,  $A_p$  is the area of the blade perpendicular to  $W$  and  $C_t$  and  $C_n$  are the tangential force coefficient and

the normal force coefficient, respectively.  $C_t$  and  $C_n$  depend on the drag and lift coefficients,  $C_d$  and  $C_l$ , and the angle of attack  $\alpha$ . [16].

The total force from the wind acting on the swept area is called the thrust force,  $F_{th}$ . It is determined as [23]:

$$F_{th} = \frac{1}{2} C_{th} \rho_{air} A V^2 \quad (2.8)$$

where  $C_{th}$  is the thrust coefficient or the drag coefficient for the whole swept area.

The gravity force,  $F_g$ , and the centrifugal load force,  $F_c$ , are both dependent on mass and defined as:

$$F_c = \sum_{i=1}^n m_i r_i \omega^2 \quad (2.9)$$

$$F_g = \sum_{i=1}^n m_i g = mg \quad (2.10)$$

where  $m_i$  is the  $i$ :th discretized element out of  $n$  elements,  $r_i$  is the radius from the axis of rotation to the mass center,  $\omega$  is the angular velocity and  $g$  is the acceleration of gravitation [21].

## 2.2 Structural modeling

Two different 3-D beam elements are available in Ansys, BEAM188 (standard in Ansys) and BEAM189. BEAM188 is a two-noded beam element while BEAM189 is a three-noded beam element. Both are based on Timoshenko beam theory [24].

Element of type BEAM188 can be based on linear, quadratic, or cubic shape functions and have one, two, or three integration points respectively. If quadratic or cubic shape functions are used, one or two internal nodes are added during the solution procedure. BEAM188 has six degrees of freedom (three translational and three rotational) at each node. Element results like strains and stresses are calculated at the element's integration points and then linearly extrapolated to the nodes. The geometry of BEAM188, together with the global coordinate

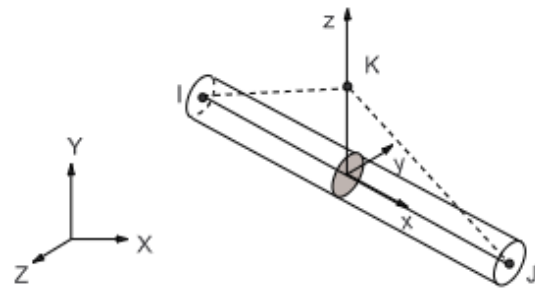


**Figure 2.4:** Geometry of a BEAM188 element, figure from Ansys help [24].

system  $(X, Y, Z)$ , the local coordinate system  $(x, y, z)$ , and the local node numbering  $(I, J, K)$  are shown in Figure 2.4 [24].

There are 12 available cross-section types in Ansys for BEAM188. Most of them are defined by their geometry, for example, rectangular, circular, and user defined. For these, the physical properties of the cross-section are not possible to modify without changing the geometry. However, the user integrated cross-section type is defined by its physical properties instead of geometry data. The physical properties that must be defined, are the area of the section,  $A_{cs}$ , the moment of inertia about the  $y$ -axis,  $I_{yy}$ , the moment of inertia around the  $z$ -axis,  $I_{zz}$  and the torsional constant,  $J$ . These must all be greater than zero. Other physical properties that can be defined are the product of inertia, the warping constant, the coordinates of the centroid, and the coordinates of the shear center. Since the actual geometry of the cross-section is not defined for user integrated cross-sections, the correct maximum and minimum stresses and strains are not given as direct outputs by Ansys [24].

The strains in a beam induced from normal forces,  $\epsilon_{xx,N}$ , and from bending moment (according to Timoshenko beam theory),  $\epsilon_{xx,B}$  can be calculated as [25, 26]:

$$\epsilon_{xx,N} = \frac{du_x}{dx} \quad (2.11)$$

$$\epsilon_{xx,B} = z \frac{\partial \phi_y}{\partial x} + y \frac{\partial \phi_z}{\partial x} = z \kappa_y + y \kappa_z \quad (2.12)$$

where  $(x, y, z)$  are the coordinates according to Figure 2.4,  $u_x$  is the deformation of the neutral axis along  $x$ ,  $\phi$  is the rotation of the cross-section and  $\kappa$  is the curvature.

The stress,  $\sigma_{xx,B}$ , and the stress range,  $\Delta\sigma_{xx,B}$ , from bending of a beam can be calculated according to Equation (2.13) and Equation (2.14):

$$\sigma_{xx,B} = \frac{M_y z}{I_{yy}} + \frac{M_z y}{I_{zz}} \quad (2.13)$$

$$\Delta\sigma_{xx,B} = 2 \sigma_{xx,B} \quad (2.14)$$

A key design criteria to consider within structural modeling is fatigue [27]. Stress is often used to determine the damage over long time, while strain is used for low cycle fatigue. For welded structures, it is important to consider the full stress range. To calculate fatigue damage, Miner's rule is commonly used. It states that the damage factor ( $D$ ) must be less than 1 divided by the design fatigue factor ( $DFF$ ). The damage factor is calculated as the sum of the total amount of cycles divided by the cycles to failure for each load case. The DFF is decided according to the standard DNVGL-RP-C203 [28]. This results in Equation (2.15) and (2.16).



$$D \leq \frac{1}{DFF} \quad (2.15)$$

$$D = \sum_{i=1}^I \frac{n_i}{N_i} \quad (2.16)$$

In Equation (2.16),  $I$  is the total number of load cases,  $n$  is the number of cycles during the lifespan for one load case and  $N$  is the number of cycles to failure for the same load case. To find  $N$  for each load case, the stress range can be calculated as described in Equation (2.14), and then utilized in an S-N curve [27] chosen according to the standard DNVGL-RP-C203 [28]. To determine  $n$  for each load case over the lifespan, the probability that the load case occurs and the time of one cycle can be used. If Equation (2.15) is not fulfilled, the structure will not last the desired lifetime and changes in the design are needed.

## 2.3 Optimization

The second major area of this project is the optimization study. While the field of optimization is vast, the focus of this project will be on parametric optimization. This will first be explained in general before the possibilities for optimization in Ansys Workbench are outlined.

### 2.3.1 General optimization theory

Optimization is a phase within a design process that can be defined as "the selection of the best design within the available means". To succeed with optimization, it is recommended to divide it into different steps, for example [29]:

1. Define the system and the design space
2. Formulate the optimization problem
3. Create a model
4. Explore the problem space
5. Solve the problem to find the optimal solution

The first task includes defining the system boundaries of the optimization. This can be done with, for example, free-body diagrams. Nothing that is outside the boundaries will be considered in the optimization but can be linked to the system as inputs or outputs. The design space can be described as everything within these boundaries [29].

The next step is to formulate the optimization problem. Normally this part consists of defining the following functions and variables [29]:

- Objective - what is the goal with the optimization?
- Design variables - what can vary throughout the optimization?
- Parameters - what are assumed to be fixed?
- Constraints - what restrictions are present?

Both the objective and the constraints must be dependent on the design variables. The objective is often expressed as a formula that should be minimized or maximized. Constraints are essential to define the design space and can in the optimization turn out to be active or inactive. An active constraint hinders the goal function from approaching a further optima while an inactive constraint does not affect the result in the end [29].

Regarding the third step, a model is a simplified description of reality. It can be physics-based models, numerical models, or data-driven models. Step four, exploring the problem space, includes, for example, ensuring that a feasible solution exists, the problem is well-bounded, and checking if the formulation of the problem can be simplified.

Finally, the last step is to solve the problem. To find the optimal solution efficiently, an appropriate optimization algorithm must be chosen. There exist plenty of optimization algorithms, but normally the methods are divided into gradient-based and non-gradient-based algorithms where the former is based on derivatives of the goal function and the latter is not. The results must then be interpreted before the optimal solution can be chosen [29].

For complex optimization problems, it is common that the amount of design variables become too many, making it difficult to accurately describe the design space. To tackle this, a design experiment, DOE, can be constructed to map the problem. A DOE is a statistical method to evaluate and optimize the performance of a system. It is an effective way of maximizing the amount of information obtained while minimizing the amount of data that needs to be collected. A full DOE often has two objectives: both lowering the number of design variables and optimizing the system [30]. It, therefore, consists of an initial part that screens the known input variables and factors affecting the system, and a final part optimizing the system's performance. To optimize the systems performance, it is common that one uses a response surface, where an algorithm creates the surface describing the design space based on a few points. This creates a more effective way of quickly mapping the problem, but can sometimes cause unreliable results if the surface is not designed correctly [24].

As stated, optimization can be done in multiple ways, and different practices within the field are constantly introduced and developed. Today, optimization is almost exclusively done through computer software and integration between FE analysis and structural optimization can be done in several different programs [31].

### 2.3.2 Optimization tools in Ansys

The focus of this project is parametric optimization, for which Ansys Workbench provides an optimization environment called the DesignXplorer. In DesignXplorer, 3 systems are relevant for this project: Direct Optimization, Parameter Correlation and Response Surface Optimization [24]. The systems can be seen in Figure 2.5.

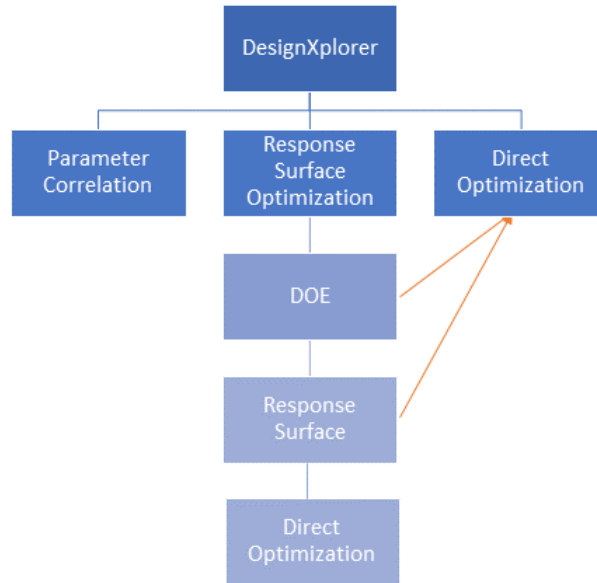


**Figure 2.5:** Outline of the DesignXplorer’s parametric optimization tools. The orange arrows indicates where connections can be created manually [24].

To handle and limit the amount of design variables, Parameter Correlation can be used. This system examines the correlation between design variables and output parameters of a model. By finding, for example, design variables with weak correlation to the important outputs, it might be possible to exclude these from the optimization. The system finds both linear and nonlinear (quadratic) associations between parameters. For linear association, Ansys have two available correlation types: Spearman and Pearson. For quadratic association, parameters are evaluated using the coefficient of determination of quadratic regression between parameters [24].

The surface optimization consists of three parts: a DOE, a response surface and an optimization. The DOE consists of different statistical techniques to sample points that will build the response surface. In Ansys, there are seven algorithms available, which are further described in the Ansys help manual [24]. In general, all algorithms try to sample points in the design space in the most time efficient way while still describing the space thoroughly. A correctly constructed DOE directly affects the

quality and accuracy of the optimization. Ansys recommends to have between 12-20 design variables for the optimization depending on the DOE type chosen [24].

The second part of the response surface optimization is called the response surface. Here, ANSYS offers six different algorithms: Genetic Aggregation, Full 2nd-order Polynomials, Kriging, Non-parametric Regression, Neural Network and Sparse Grid. Ansys recommends initial usage of genetic aggregation, but since this is a time consuming method, it is recommended to try the full 2nd-order polynomials, Kriging and Non-parametric Regression in that order if Genetic Aggregation does not achieve accurate results. Neural Network and Sparse Grid is only recommended in very specific cases. Furthermore, a surface can be refined for better result without changing the surface method, which is described further in the Ansys help manual [24]. It is not recommended to have more than 10-15 design variables when creating a surface [24].

Finally, the last part of the optimization tool is the optimization algorithms, which can be used with a DOE, on a response surface or in the direct optimization environment. The algorithms available in Ansys are Shifted Hammersley Sampling (Screening), Multi-Objective Genetic Algorithm (MOGA), Nonlinear Programming by Quadratic Lagrangian (NLPQL), Mixed-Integer Sequential Quadratic Programming (MISQP), Adaptive Single-Objective Optimization (ASO) and Adaptive Multiple-Objective Optimization (AMO). More information about these can be found in the Ansys help manual [24].

## 2.4 Cost analysis

The optimal wind turbine can be considered to be the least costly turbine that is structurally sound and with good aerodynamic performance and efficiency. The price of a wind turbine is a complex calculation, as different costs spanning over the full lifetime of the product must be taken into account. The efficiency and energy production of the structure must also be considered to provide an accurate cost estimation. Therefore, it is standard practice to describe the cost of a VAWT through the Levelized cost of energy, LCOE [32].

### 2.4.1 LCOE

LCOE can be described as the cost of building and operating an energy-generating asset per unit of total energy generated over an assumed lifetime. It is commonly used as a measurement to compare and assess different methods of energy production, and considers all life cycle costs of a project [33]. The standard formula for LCOE is:

$$LCOE = \frac{CAPEX + OPEX}{AEP} \quad (2.17)$$

where AEP stands for annual energy production, and can be estimated for a VAWT by looking at site characteristics, turbine energy conversion and wind turbine farm energy conversion [34].

CAPEX stands for capital expenses and expenditures and contains the money spent by a company to buy or improve fixed assets [35]. In the context of a VAWT project, it often refers to the costs associated with the initial investments made before the VAWT is operating and fully functional. This includes, for example, purchasing, administrative and installation costs [8].

OPEX stands for operating expenditures and contains the money spent by a company during ordinary operations. This can refer to insurance, annual fees, general administration and management & maintenance [36].

### 2.4.2 FVAWT costs

CAPEX and OPEX of a FVAWT can be further distinguished as suggested by Sandia National Laboratories [8], where the cost of FVAWT has been divided into three main categories: operation and maintenance, O&M, balance of system costs, and turbine capital costs. The first refers to OPEX while the two later fall mainly into the category of CAPEX. Balance of system contains costs for transportation, installation, electrical interconnection, transmission, and other similar costs. Turbine capital costs include, for example, the support structure, drive-train costs, control and monitoring system costs, marinization costs, and rotor costs [8]. An outline of this division can be seen in Figure 2.6.

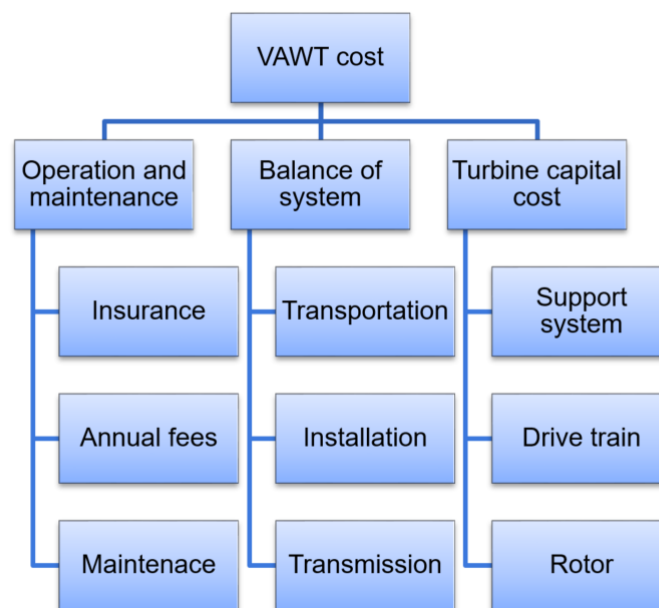


**Figure 2.6:** Outline of the cost for a FVAWT as described by Sandia National Laboratories [8].

For most offshore projects, O&M costs are estimated to comprise 20-30% of the total life cycle costs. Currently, it is most common to decrease this cost by improving HAWT technology, however, studies show that the FVAWT concept has an inherent ability to lower this cost [8]. O&M is heavily affected by the placement of the wind turbine [33].

The cost of balance of systems is also dependent on the location site and can be difficult to estimate. For example, each site for a wind farm might have unique requirements for installation, and there is a great variation in installation methods that can be chosen from [37]. Transmission costs are also a major issue in wind energy development overall, as the best spots for wind energy generation are not always close to the places where the electricity is used [33].

Regarding the turbine capital costs, the material, manufacturing and production costs of all parts must be considered. For the support structure, the sparbuoy is regarded as one of the best options in economic terms [38]. For the rotor costs, there are three different parts considered for an H-rotor turbine: the struts, the blades, and the tower. For each of these, material costs and costs related to manufacturing should be considered. Overall, the design of the rotor affects the costs greatly. Most noticeably, the shape of the blades has a great impact on the manufacturing costs, as more angled or curved blades are significantly harder to manufacture than straight blades. Furthermore, the material used for all three parts heavily affects the costs. For struts and blades, it is common to use some form of glass or carbon composite material while the tower is usually formed by steel. In earlier studies, the rotor, which is the focus of this project, is estimated to stand for about 28% of the total life-cycle cost [8].

# 3

## Methodology

In this section, the project work conducted to reach the two aims of the thesis is described. The project can be divided in three main parts; Literature study, testing phase and optimization of concepts.

In the literature study, general theory about FVAWT, FE modelling and optimization were studied together with specific information and data concerning SeaTwirl's wind turbine. Furthermore, the possibilities of the software Ansys Workbench was part of the study. Most of the study was conducted during the initial phase of the project.

Based on the literature study, several tests were conducted to obtain the optimization method described in Section 4. Creating this method was the first aim of the project stated in Section 1.2. The test phase included trials regarding FE model construction, identification of relevant assumptions, optimization problem definition, and tests of optimization strategies. Since all tasks affected each other, an iterative approach was used. Starting with a basic model of only two struts and a blade, the complexity of the models were increased successively. Further tests were then conducted on each model. While an H-rotor design was used, the goal was to construct a general method that could be utilized on other concepts.

In the last phase, the results from the literature study and the conducted tests were combined into the optimization method. The method was then utilized on four concepts. During this phase, the up-scaling of the 1 MW rotor to a 10 MW rotor was a main task. The results of the optimizations were analysed to fulfill the second aim of the project, but also to verify that the optimization method worked as expected.

Ansys Workbench was used as the main tool during the project. The geometry was defined in DesignModeler and the static and modal analyses were performed in Ansys Mechanical. The Microsoft Office Excel system in Ansys was used to define inputs and calculate parameters. Parameters and design variables were sent both from Ansys Workbench to Excel and vice versa. Ansys DesignXploration was used for the optimization.





# 4

## Optimization method

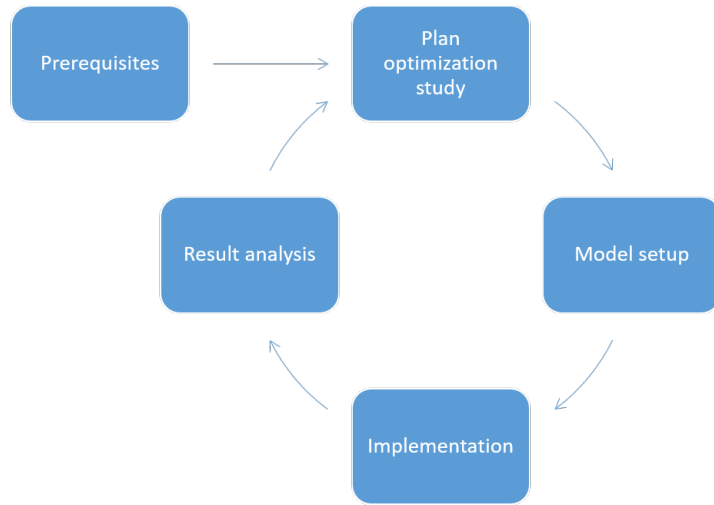


**Figure 4.1:** Description of the full evaluation method developed for H-rotor designs.

This section will outline the general method constructed to evaluate the concepts in this project and reach the first goal of the study. Although the scope only contains the examination of an H-rotor design, the general work flow could potentially be used for several vertical axis turbine or rotor designs. The method should be used for effective concept evaluation at an early design stage within the product development process as described in Section 1.1.2. This indicates that the method must be usable when little is known regarding the concepts, be time-efficient to use on several concepts and still give reliable results. The previous and following steps of the product development process is outside of the scope of this project. However, within optimization, concept generation is naturally included as design points are generated to find an optimal design. It could furthermore be argued that the method could be used for evaluation without including the optimization scope. However, as little is known of the initial design, optimization was used as part of the evaluation to give fair results when concepts are compared.

The general goal of this method is to evaluate a concept and find the optimal version between different type of designs. The method should be adapted both to compare two entirely different concepts by applying the method separately, but also to identify which design of a specific concept that is ideal. With these requirements

in mind, five steps have been identified. An outline of these five steps and their content is listed in Table 4.1. To obtain a fully optimized model, it is recommended to conduct the method several times as results are obtained and analysed, as is described in Figure 4.1.

Prerequisites	<ul style="list-style-type: none"> <li>- Aerodynamic loads on blades</li> <li>- Complete concept generation</li> <li>- Define tools</li> </ul>
Plan optimization study	<ul style="list-style-type: none"> <li>- Identify objective</li> <li>- Identify and prioritize design variables</li> <li>- Identify fixed parameters</li> <li>- Identify and prioritize constraints</li> </ul>
Model setup	<ul style="list-style-type: none"> <li>- Define goal function formula</li> <li>- Define constraints</li> <li>- Define upper and lower values for design variables</li> <li>- Finalize FE-model</li> <li>- Decide on optimization flow</li> </ul>
Implementation	<ul style="list-style-type: none"> <li>- Run planned study</li> </ul>
Result analysis	<ul style="list-style-type: none"> <li>- Are the results reliable?</li> <li>- Was the optimization setup reasonable?</li> <li>- What conclusions can be drawn?</li> <li>- Can the process be improved?</li> </ul>

**Table 4.1:** Outline of the constructed method for evaluation of H-rotors.

The first step is to complete the prerequisites. To be able to apply aerodynamic loads on the blades in the FE model, some knowledge about these must be present. Ideally, the aerodynamic loads would be known for all the designs, including those with different aspect ratio and chord length, that are evaluated during the optimization. This is often not possible in an early design phase. Instead, the aerodynamic loads from one reference design is scaled, which is further discussed in Section 5.5.2, when the design is changed during the optimization. These loads can be obtained in different ways, e.g. by real tests, load simulations, analytical calculations or estimations based on other concepts. Furthermore, which concepts that should be evaluated, and their initial design, must be identified. Here, it is important to remember that the method does take time and should not be used for all initial ideas. Optimization and FE-modeling environment and tools must also be decided as a prerequisite.

The second step of the method is to plan the optimization study. This can be done in a similar way as described in Section 2.3. An important part of this step is to

identify and prioritize the design variables . Most times, there are more parameters that could be set as design variables than it is possible to include in the optimization. Similarly, it is also not feasible to consider all possible constraints within a reasonable time-frame. Therefore, the fixed parameters, design variables and constraints should be chosen with regards to the goal function and prioritized through discussions and previous studies.

The third step is the model setup, where the FE-model should be built according to the specifications and plans from the previous steps. The optimization should also be constructed by calculating constraints and the goal function. Further, the upper and lower boundaries of the design variables should be decided through, for example, results from previous studies, or boundaries caused by the model constructed. Optimization opportunities within the tool chosen should be investigated and a workflow decided.

Finally, the model should be implemented and the results analysed according to the questions stated in Table 4.1. Based on the analysis, this method should then be used iteratively together with a concept generation phase. After each completed and analysed simulation, new possible improvements or concepts should be identified to be run through the method again, as visualized in Figure 4.1.



# 5

## H-rotor setup

This section contains steps one to three of the outlined method in the previous chapter. The method is tested on an H-rotor based on the current design of the SeaTwirl S2X model.

### 5.1 Prerequisites

As mentioned in Section 4, three major prerequisites were needed at the start of the project. This section describes the data that were used as input to define these.

#### 5.1.1 The concept of a VAWT with H-rotor

All the concepts studied in this project were based on the design of SeaTwirl's S2X, which is shown in Figure 5.1. S2X is a VAWT of H-rotor type with straight blades, SB-VAWT. The rotor consists of 3 blades connected to a tower by two struts each. The blades have NACA0018 profile while the struts go from circular profiles closest to the tower to NACA0028 profiles closest to the blades. In the current design of S2X, the connections between blades and struts are fixed. Hubs are connecting the struts to tower. The struts and blades consist of carbon-fiber composite material and the material in the tower is steel.

The tower is connected to a generator housing, a mooring system, and a sub-sea support structure consisting of a sparbuoy. As the wind causes the rotor to rotate, so does the tower and the sub-sea part. The sparbuoy is used to create stability and counter the over-turning moment, similar to the function of a keel on a sailboat. The sparbuoy consists of 3 parts: at the top, there is an air compartment, right below is a compartment that can either be water or air-filled and the last part consists of

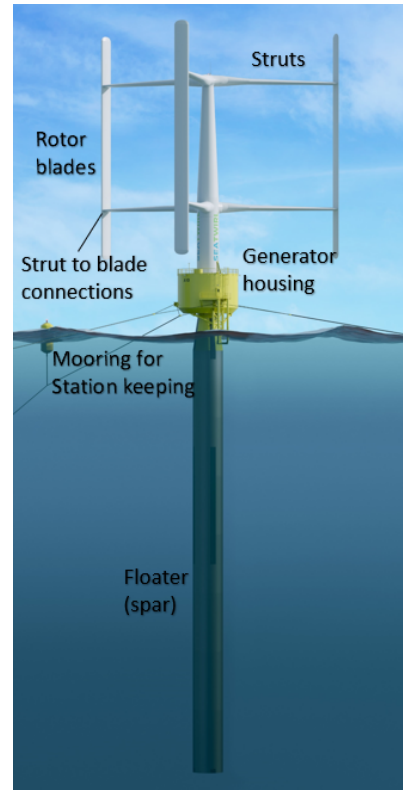


**Figure 5.1:** Breakdown of the parts of Seatwirl's current FVAWT design, the S2X [15].

a solid ballast of MagnaDense. MagnaDense is a high-density aggregate, used as heavyweight ballast in many applications.

Based on SeaTwirl's S2X, four concepts were optimized separately in this study:

- **1 MW fixed:** The same global dimensions and the same blade to strut connection (fixed) as S2X.
- **1 MW pinned:** The same global dimensions as S2X but with a pinned blade to strut connection.
- **10 MW fixed:** The 1 MW fixed concept up-scaled by increasing the area according to Equation (2.2).
- **10 MW pinned:** The 1 MW pinned concept up-scaled by increasing the area according to Equation (2.2).

### 5.1.2 Load analysis

The necessary information about aerodynamic loads on blades according to Section 4, was obtained from an existing global load analysis of the S2X, performed by Principia. The load analysis included wind and wave loads applied on the full S2X wind turbine, the model is shown in Figure 5.2 Simulations were performed for different wind speeds (2, 4, 6, 8, 10, 12, 14, 16, 18, and 20 m/s) and each simulation contained outputs at each simulated time step.

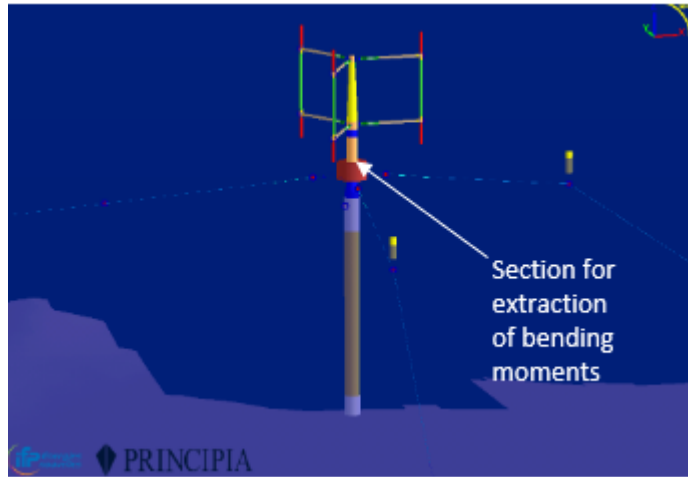


**Figure 5.2:** Global model from the Principia analysis.

The loads giving the largest axial compression and tension, respectively, in one strut to blade connection were brought from SeaTwirl. These loads were assumed to be the most crucial ones and were taken at two-time steps at a wind speed of 20 m/s. Bending moments used in the fatigue analysis, see , were extracted for each wind speed simulated in the Principia analysis in each tower section according to Figure 5.2.

### 5.1.3 Tools used in the optimization

As described in Section 1.2, Ansys Workbench was the major tool used in the project. For geometry creation, DesignModeler was used and for optimization, the tools in DesignXplorer were used. To get a better overview of parameters and define relations

between parameters, the Excel add-in of Ansys was used. Comparing different tools was not part of the scope of this project, hence the choice of tools was made early in the project, and based on that SeaTwirl uses Ansys.

## 5.2 Goal function

As discussed in Section 2.4, the optimal wind turbine is often considered to be the one that has the lowest cost while remaining structurally sound and with good aerodynamic performance and efficiency. For this project and optimization, it was therefore reasonable to construct a goal function related to cost. As mentioned in the Section 2.4, there are several factors that affect the cost of the overall structure. However, it was not reasonable to estimate the full LCOE within the scope of this project, as it was conducted for an early stage of development, and the focus was on the rotor. Therefore, several parameters regarding cost were disregarded. To begin with, it is difficult to correctly estimate the OPEX costs of a FVAWT at an initial state of the design and it was therefore neglected. In addition, the balance of system costs were not considered, as these were not directly related to the rotor. Finally, within the category of turbine cost; drive-train costs, control and monitoring system costs and marinization costs were not considered as these were deemed to be outside of the scope. In short, only costs associated to the rotor and support structure were taken into account. As the rotor cost stands for about 28% of the total life-cycle cost of the turbine, also mentioned in Section 2.4, this remained a relevant cost analysis for the FVAWT designs discussed.

The rotor cost is heavily affected by the shape of the blades and the material cost of the structure, as mentioned in Section 2.4. However, as this project was focused only on straight bladed H-rotor designs, this cost was disregarded. Lowering the amount of material used was, within the limits of this projects scope, the major way to minimize the material cost. This was approached by trying to lower the mass of the rotor, as this lead to a lower material cost for the rotor parts.

For the support structure costs, optimization of the sparbuoy itself was outside of the scope of the project. This cost was only considered as a change in rotor might lead to a more stable structure, and a cheaper sparbuoy. Therefore, the focus was solely consisted of reducing the amount of material of the sparbuoy through optimizing on the rotor. For this two main parameters were relevant: the mass of the rotor and the vertical centre of gravity (VCoG). Lowering any of these will enable the use of a lighter sparbuoy, without endangering the stability of the structure.

To construct a goal function related to the cost of the product, the mass and the vertical centre of gravity of the FVAWT were considered. However, the material of the parts of the rotor (the strut, blade and tower) were not the same in the chosen concepts, and therefore have different costs per kilogram. The same was true for the material of the sparbuoy. Hence, lowering the mass of these parts should not have the same effect on the goal function, as this would not capture the true cost reduction. Instead, the goal function took the mass of the strut, blade and tower

as well as the total VCoG of the rotor into consideration separately and weighted these according to the cost of material for each part. The full formula for the goal function can be seen in Equation (5.1):

$$G = K_1 \cdot m_{\text{strut1}} + K_1 \cdot m_{\text{strut1}} + K_2 \cdot m_{\text{tower}} + K_3 \cdot m_{\text{blade}} + K_4 \cdot VCoG_{\text{tot}} \quad (5.1)$$

To find the weights ( $K$ ), a sensitivity analysis was constructed. The analysis was performed by testing how the cost was affected by lowering the mass or VCoG of the different parts of the rotor by one unit. In this case, 1 mTon for each part and 1 m from the full rotor VCoG was reduced separately and the cost effect for each parameter plotted against each other. The relationships was assumed to be linear based on the found data. The k-value for each slope was calculated and the highest value set as a reference point by which all k-values were divided by. These numbers were then set as the final K value for each variable in the equation above.

When calculating the cost of the sparbuoy, a formula determining how much of the weight of the sparbuoy that could be reduced as the mass or VCoG of the rotor is lowered must be constructed. It was also important to decide which part of the sparbuoy, out of the ones mentioned in Section 1.1.3, that should be lowered as the rotor was optimized. Regarding the first issue, Equation (5.2) shows the relationship between rotor optimization and sparbuoy mass:

$$C = (COB_{\text{tot}} - VCOG_{\text{tot}}) \cdot m_{\text{tot}} \quad (5.2)$$

Equation (5.2) is based on the righting moment of a turbine and gives a general idea of the stability of the structure. The parameter  $C$  was kept as a constant as the rotor design changes. For the second issue, it was assumed that only the solid ballast, mentioned in 1.1.3, was taken away when the rotor was optimized. The shape, thickness and other parameters of the sparbuoy were set as constant. The draft was also set to a constant. The cost of sparbuoy steel was used rather than the cost of solid ballast, as this would give a more accurate cost weight for the VCoG.

### 5.3 Constraints

As discussed in Section 2.3, optimization problems normally contain constraints that restrict the problem. In this project, constraints were defined for the eigenfrequency, the maximum allowed strain in the blades and the struts, and the fatigue life of the tower.



### 5.3.1 Eigenfrequency

A constraint was defined to ensure that the first natural eigenfrequency of the rotor did not coincide with the 1P or 3P frequency, see Section 2.1.1. The first eigenfrequency of the S2X was well above the 3P frequency. Hence the requirement was implemented by constraining the first eigenfrequency to be equal to or larger than the 3P frequency times a safety margin of 1.1. The first eigenfrequency was calculated by the mechanical modal analysis in Ansys.

### 5.3.2 Strain

An ULS of a maximum 0.2% strain was used as a design criterion for the composite material in the blades and the struts. This is a conservative constraint since it will imply eternal life. Since user integrated cross-sections were used for the struts and blades, the strains were not given as an output automatically in Ansys. Therefore an Ansys extension was created to calculate the strains. Four scripts were created, calculating the maximum and minimum total strain in the struts and blades, respectively. The total strain was calculated in Python scripts where  $\epsilon_{xx,N}$ , according to Equation (2.11), and  $\epsilon_{xx,B}$ , according to Equation (2.12), were summed together.  $\epsilon_{xx,N}$  was determined directly by the user defined result SMISC7 while  $\epsilon_{xx,B}$  was calculated from the curvatures, determined by the user defined results SMISC8 and SMISC9, see Ansys help for more information about scripting in Ansys [24]. To simplify the script, the strains were only calculated at the leading edge, the trailing edge, and the points of the maximum thickness of the cross-section according to Figure 5.3. The scripts also considered an increased chord length due to a change of rotor radius, described in Section 5.5.2. To define the strains as user defined results and to be able to parameterize them in Ansys Mechanical, an xml script was created. The extension, consisting of the Python scripts and the xml script, was verified by an analysis of a cantilever beam with a rectangular cross-section. The strains calculated by the extensions were compared with the strains available as results for beams with predefined cross-sections in Ansys.

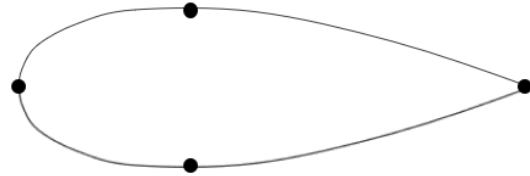


**Figure 5.3:** The black points marks the places at which the strains were calculate for the blades and the struts.

### 5.3.3 Fatigue

For offshore structures, it is relevant to consider the fatigue and buckling effects on the structure, and set constraints with regards to these [27]. It was decided to not include buckling within the scope of this project due to its complexity. Regarding fatigue, the scope was limited to include only the thrust force,  $F_{th}$ , on the tower and the bending moment,  $M_{th}$  this thrust force causes, which can be calculated as follows.

$$M_{th} = F_{th} \left( \frac{L_{blade}}{2} + L_{bts} \right) \quad (5.3)$$

Where  $L_{bts}$  is the distance from the bottom of the blade to the sea level. To fully describe the fatigue effect of  $F_{th}$ , one must look at the full lifetime of the FVAWT, which in this analysis was set to 25 years. The moment must also be calculated for each load case occurring during this timespan, which in this project was limited to the 10 load cases from the Principia studies. Equation (2.8) was utilized to calculate  $F_{th}$  for each load case. The values for the different wind speeds and  $C_d$  used in this analysis was obtained from the Principia studies and can be seen in Appendix B. The analytical bending moments for each load case determined from Equation (5.3) were compared to those obtained from the Principia studies described in Section 5.1 for the 1 MW. As the differences were deemed insignificant, the analytical results were used for both the 1 and 10 MW rotors.

Thereafter, a fatigue analysis as described in Section 2.2 was performed by first calculating the stress range according to Equation (2.14). One cycle was defined as one rotation of the rotor. The DFF was set to two and a D type S-N curve was chosen according to the standard DNVGL-RP-C203 [28]. The chosen value for the blade length,  $L_{blade}$ , outer radius of the tower,  $R_o$ , and inner radius of the tower,  $R_i$ , will be discussed in Section 5.4.

## 5.4 Parameters and design variables

Defining parameters and design variables are an important part of the optimization procedure, as discussed in Section 4. The parameters and design variables considered in this project are defined in this section. The initial values of design variables and the values for fixed parameters were in general based on the S2X. For the 10 MW concept, parameters were in most cases linearly scaled in the same way as the geometry was to obtain the required sweep area,  $A$ . All the inputs to the optimizations can be seen in section 6.1.

### 5.4.1 Strut

The strut design variables were the vertical attachment position to the tower, the vertical inclination of the struts, the cross-section properties, and the length. The vertical position and the angle were optimized by two design variables,  $AP_{strut,i,p}$  and  $I_{strut,i,p}$  where index  $i = 1, 2$  is the lower or upper strut.  $AP_{strut,i,p}$  and  $I_{strut,i,p}$  were dimensionless design variables allowed to vary between 0 and 1. A change in  $AP_{strut,i,p}$  implied a vertical displacement of point  $AP_{strut,i}$  closest to the tower, according to Figure 5.4. A change in  $I_{strut,i,p}$  defined a relative vertical displacement of point  $I_{strut,i}$  compared to point  $AP_{strut,i}$ , according to Figure 5.4. Hence, the vertical attachment position to the tower was dependent on  $AP_{strut,i,p}$  while the inclination of the strut, and subsequently its attachment position to the blade, was

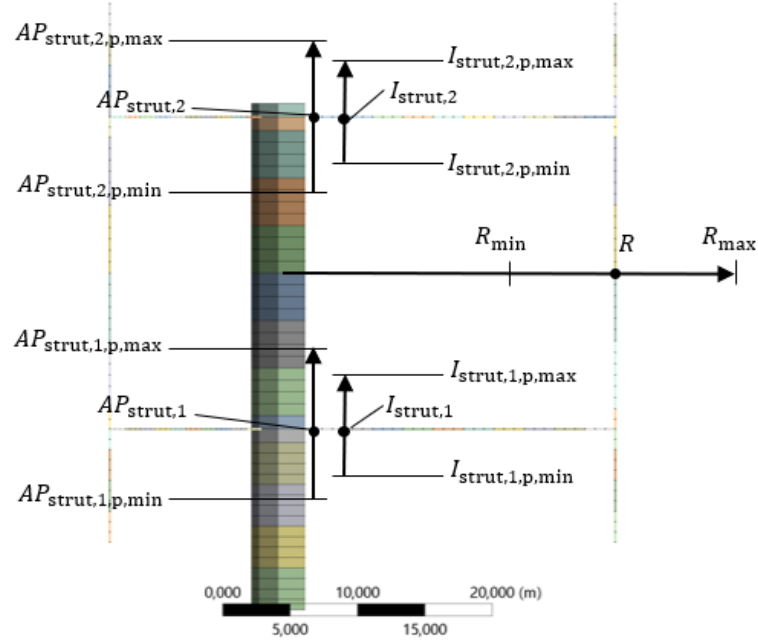


**Figure 5.4:** The design variables affecting the geometry of the rotor. The black dots are located at the initial positions and the arrows show how the dots can vary depending on the values of the design variables.

dependent on  $I_{\text{strut},i,p}$ . The limit of point  $AP_{\text{strut},i,p}$  was defined by a maximum allowed displacement from the initial position while the limit of point  $I_{\text{strut},i}$  was defined by a maximum allowed inclination in degrees. The struts were initially placed at 21% and 79% of the blade length, according to the information stated in Section 2.1.1.

The length of the struts was defined as the radius of the rotor,  $R$ , minus the length of the connections to the tower. The radius was a design variable, see Figure 5.4, with limits set to satisfy the condition of rotor aspect ratio between 0.5 and 2, see Section 2.1.1. The length of the connections was defined as an input that was kept constant during the optimization.

The cross-section properties were optimized by one design variable,  $CS_{\text{strut}}$  for each strut section. This design variable is described in Section 5.5.1.

## 5.4.2 Blade

Blade parameters considered during the optimization were the blade length, the attachment position of the struts, and the cross-section properties. The blade length was defined as  $A/R$ . Hence it was dependent on the design variable  $R$  and not a design variable itself. Nor was the attachment positions to the struts design variables themselves since they depended on  $AP_{\text{strut},i,p}$  and  $I_{\text{strut},i,p}$ . Consequently, the only independent design variables of the blades were those optimizing the cross-section properties. One design variable,  $CS_{\text{blade}}$ , was defined for each blade section.

### 5.4.3 Tower

For the tower, three relevant parameters were considered: The height  $L_{\text{tower}}$ , the outer radius,  $R_o$  and the inner radius,  $R_i$ . The height of the tower was set as dependent on the attachment position of the upper strut, as this is the main variable that governs the tower height for the concepts chosen. In the original layout of the SeaTwirl S2X, the tower is tapered with a varying inner and outer radius along the tower length. To limit the number of design variables and enable more focus on the strut and blade optimization, the tower was instead set as a cylinder with constant inner and outer radius along the full length. Furthermore, since buckling was excluded from the scope, it was decided that optimizing the outer radius of the tower would not lead to feasible concepts.  $R_o$  was therefore set as a fixed parameter according to the current S2X design. The only varying parameter was then the inner radius of the tower, which was allowed to take on values governed by a fatigue constraint.

A fatigue analysis according to Section 5.3.3 was performed outside of the optimization tool. By rewriting Equation (2.13), Equation (5.3) and the formula for second moment of area of a tube section <sup>1</sup>, the expression of  $R_i$  is as follows,

$$R_i = \sqrt[4]{R_o^4 - \frac{F_{\text{th}} \cdot (\frac{L_{\text{blade}}}{2} + L_{\text{bts}}) \cdot R_o}{\sigma} \cdot \frac{4}{\pi}} \quad (5.4)$$

In the optimization, this expression was used for the inner radius, with the only parameter allowed to vary being the length of the blade. To find the value for the stress amplitude in Equation (5.4), the fatigue analysis described in Section 2.2 and Section 5.3.3 was conducted for several different values of the inner radius. All other values were set according to the initial geometry of the concept. This approach gave the minimum initial thickness that fulfills the requirement in Equation (2.15). Finally, the stress value for one load case was chosen and these variables put in as constants in Equation (5.4) to calculate  $R_i$ . All values for the 1 and 10 MW can be found in Section 6.1. It is important to highlight that with this approach, the length of the blade was the parameter governing the thickness of the tower, rather than it being optimized directly.

### 5.4.4 Further parameters

The swept area of the rotor,  $A$ , was calculated from Equation (2.2), while the other parameters in the Equation (2.2) were defined as inputs to the model.  $P$  is the power output extracted from the wind; where 1 MW or 10 MW were used for the different concepts.  $V_{\text{rated}}$  is a rated wind speed,  $V_{\text{rated}}$ , in which the rotor is designed to perform optimal. A  $V_{\text{rated}}$  of 12.7 m/s was used since it was estimated to be a reasonable wind speed at possible operation locations. As discussed in Section 2.1.1,  $C_p$  normally lies around 0.4 for VAWT, hence it was also used in this study.

---

<sup>1</sup>  $I_{yy} = \frac{\pi}{4} \cdot (R_o^4 - R_i^4)$

To be able to calculate  $\omega$  from Equation (2.3),  $\lambda$  must be given. As discussed in Section 2.1.1, a constant  $s\lambda^3$  will give a constant  $C_p$ . In this project,  $s$  was kept constant during the optimization and hence also  $\lambda$ . The value of  $\lambda$  was based on S2X and the same value was used for both the 1 MW concept and the 10 MW concept.

## 5.5 Modelling

To properly construct the FE-model with regards to the design variables, parameters and constraints discussed, several aspects had to be taken into account. The beam model created in Ansys had to be developed such that several optimization possibilities could, later on, be tested.

### 5.5.1 Cross-section properties

Most of the blades and struts in S2X have NACA profiles. For simplicity, NACA profiles were used for the whole blades and struts in this study. There is no available cross-section type for NACA profiles in Ansys. Furthermore, the blades and the struts in S2X are made of composite material, implying anisotropic material behaviour and cross-section properties dependent on the layup of the laminate. Hence, user integrated cross-sections were used, for which the cross-section properties are defined manually.

As discussed in Section 2.2,  $A_{cs}$ ,  $I_{yy}$ ,  $I_{zz}$  and  $J$  must be defined for a beam cross-section and these were the cross-section properties considered in this study. These properties depend on multiple parameters. However, only two out of these parameters, the thickness of the laminate,  $t_l$ , and the chord length,  $c$ , were allowed to vary during the optimization.

To optimize on the cross-section properties, it was therefore essential to determine how the cross-section properties ( $A_{cs}$ ,  $I_{yy}$ ,  $I_{zz}$  and  $J$ ) vary with  $t_l$  and  $c$ , respectively. Initially  $c$  was kept constant to find the relationship between the cross-section properties and  $t_l$ .  $A_{cs}$ ,  $I_{yy}$ ,  $I_{zz}$  and  $J$  were then plotted versus  $t_l$  for a standard NACA profile. From the result of these plots, linear relations between the properties and  $t_l$  were considered to be good approximations:

$$A_{cs}(t_l) \propto I_{yy}(t_l) \propto I_{zz}(t_l) \propto J(t_l) \propto \frac{t_l}{t_{l,ini}} \quad (5.5)$$

where  $t_{l,ini}$  is the initial thickness.

When the chord length is changed but the thickness is kept constant, the properties are scaled differently compared to when the thickness is changed.  $A_{cs}$  is proportional to  $c^2$  while  $I_{yy}$ ,  $I_{zz}$  and  $J$  are proportional to  $c^4$ . The cross-section properties' dependence on  $c$  can be summarized as:

$$A_{cs}(c) \propto \frac{c^2}{c_{ini}^2} \quad (5.6)$$

$$I_{yy}(c) \propto I_{zz}(c) \propto J(c) \propto \frac{c^4}{c_{ini}^4} \quad (5.7)$$

where  $c_{ini}$  is a chosen initial value of  $c$ .

As mentioned in Section 2.3, it is important to limit the number of design variables. Having four different design variables for  $A_{cs}$ ,  $I_{yy}$ ,  $I_{zz}$  and  $J$  was therefore not an option. To circumvent this, relations were determined between the cross-section properties, resulting in that  $I_{yy}$ ,  $I_{zz}$  and  $J$  could be written as linear functions of  $A_{cs}$ :

$$I_{yy} = K_{I_{yy}} A_{cs} \quad (5.8)$$

$$I_{zz} = K_{I_{zz}} A_{cs} \quad (5.9)$$

$$J = K_J A_{cs} \quad (5.10)$$

where  $K_{I_{yy}}$ ,  $K_{I_{zz}}$  and  $K_J$  are constants. These relations were determined from S2X. The relations for the blades were taken as the average relation of all blade sections. Since the struts in S2X vary from circular profiles to NACA profiles, this relation was determined as the average relation of the sections with NACA profile, i.e. the sections closest to the blade.

Finally, by combining Equation (5.5)-(5.10), all cross-section properties could be written as functions of the initial cross-section area,  $A_{cs,ini}$  and one design variable could be used to optimize on all the cross-section properties:

$$A_{cs} = \frac{t_l}{t_{l,ini}} \frac{c^2}{c_{ini}^2} A_{cs,ini} = CS \frac{R_{ini}^2}{R^2} A_{cs,ini} \quad (5.11)$$

$$I_{yy} = \frac{t_l}{t_{l,ini}} \frac{c^4}{c_{ini}^4} K_{I_{yy}} A_{cs,ini} = CS K_{I_{yy}} A_{cs,ini} \quad (5.12)$$

$$I_{zz} = \frac{t_l}{t_{l,ini}} \frac{c^4}{c_{ini}^4} K_{I_{zz}} A_{cs,ini} = CS K_{I_{zz}} A_{cs,ini} \quad (5.13)$$

$$J = \frac{t_l}{t_{l,ini}} \frac{c^4}{c_{ini}^4} K_J A_{cs,ini} = CS K_J A_{cs,ini} \quad (5.14)$$

where  $CS = t_l/t_{l,ini} (c/c_{ini})^4 A_{cs,ini} = t_l/t_{l,ini} (R/R_{ini})^4 A_{cs,ini}$  is a combined design variable, with the assumption that  $c$  is linearly dependent on  $R$ , as described in Section 5.5.2.

The initial values of the cross-section properties of the blades and the struts were based on SeaTwirl's values from NuMAD, a tool for designing wind turbine blades. The outputs from NuMAD were the stiffness properties  $EI_{yy}$ ,  $EI_{zz}$ ,  $GJ$ , and  $EA$ . These values were recalculated to the cross-section properties needed in Ansys by assuming a simple linear elastic material with Young's modulus 1 GPa and Poisson's ratio 0.3.

### 5.5.2 Loads and boundary conditions

To calculate the loads for wind turbines with different sizes and power outputs, a reasonable way to scale the loads had to be found. Hence the Principia loads were analysed. The minimum, maximum, and average tangential forces from the Principia load analysis are shown for different wind speeds in Figure 5.5. It can be seen that the average tangential force,  $\bar{F}_t$  is almost constant at wind speeds above the rated wind speed (12.7 m/s). It was hence assumed that the crucial load cases could be scaled from  $\bar{F}_t$  at rated wind speed.

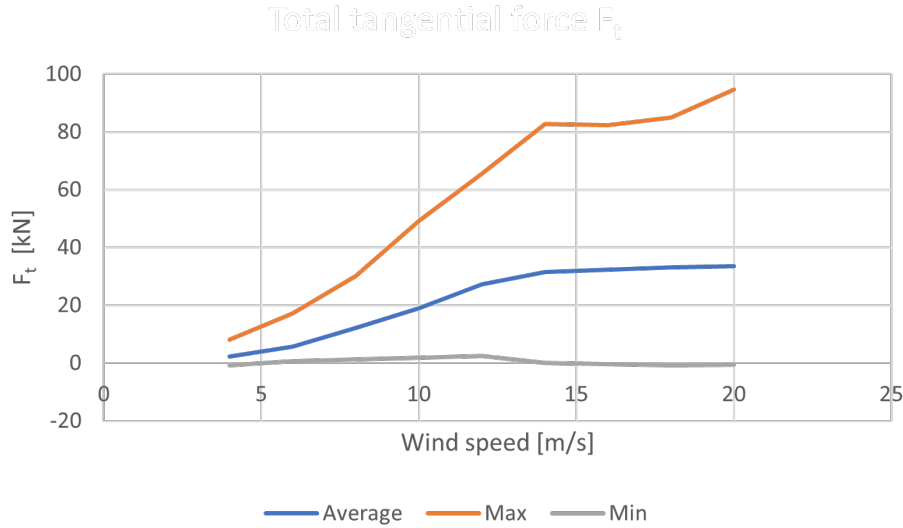


**Figure 5.5:** Average, maximum, and minimum tangential force for different wind speeds.

Furthermore, it was important to ensure that the loads stayed reasonable as the design was changed during the optimization. The  $\bar{F}_t$  needed to extract the wanted  $P$  can be calculated according to Equation (2.5):

$$\bar{F}_t = \frac{P}{NR\omega} = \frac{P}{R(v/R)} = \frac{P}{V\lambda} \quad (5.15)$$

where it can be seen that the required  $\bar{F}_t$  does not change with the radius as long as the wind speed,  $V$ , and the tip speed ratio,  $\lambda$ , are constant. Hence, the required  $\bar{F}_t$  is assumed to be constant during the optimization since  $V_{\text{rated}}$

and  $\lambda_{\text{rated}}$  are constant. However, since the length of the blades is inversely proportional to  $R$ , the area in Equation (2.6) is also inversely proportional to  $R$ . To compensate for this and achieve the required  $\bar{F}_t$ , the assumed chord length was scaled linearly with  $R$  to keep  $A_p$  constant. Scaling  $c$  linearly with  $R$  will give a constant  $s$ , see Equation (2.1), and hence also a constant relation between  $s$  and  $\lambda$ , see Section 2.1.1.

The aerodynamic loads were applied as forces on the edge of the blades in Ansys. Hence the load was evenly distributed over the length of a blade and the total magnitude of the force on one blade was kept constant even if the length of the blade was changed.

The Ansys load types Standard Earth Gravity and Rotational Velocity were used to apply gravity loads and centrifugal loads, respectively. Since a constant tip speed ratio was assumed when the radius varied, the angular velocity was a function of  $R$  according to Equation (2.3). A fixed boundary condition was applied at the bottom of the tower. The applied loads and the fixed boundary condition are shown in Figure 5.6.

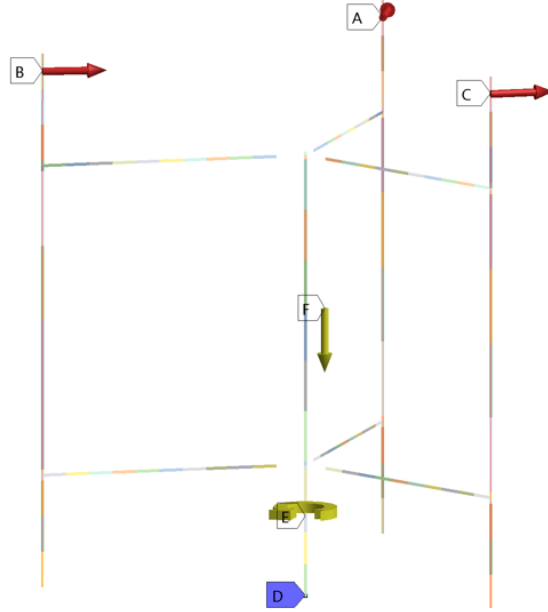


**Figure 5.6:** Loads applied on the FE model. A, B, and C represents the aerodynamic loads, E represents the centrifugal force, F represents the gravitational force and D shows the fixed boundary condition.

### 5.5.3 Coordinate systems

Different Cartesian coordinate systems are used in the FE model to facilitate the analyses. Cross-sections are defined in different planes in Ansys DesignModeler (xy-plane) and Ansys Mechanical (yz-plane), which is shown in Figure 5.7 [24]. This is not affecting the analyses and hence the yz-plane will always be used to define parameters, results, and coordinate systems for cross-sections in this report. To orient the cross-sections correctly, Cross-Section Alignment was used in DesignModeler. A blade toe-out, rotation of the blade about its axial axis, of  $2^\circ$  was also defined by the Cross-Section Alignment

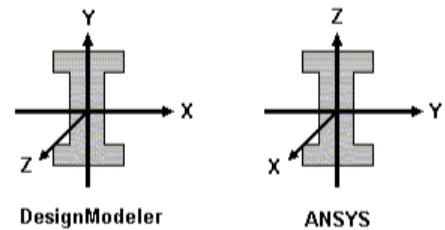


**Figure 5.7:** Coordinate systems for cross-sections in Design Modeler and Ansys, figure taken from Ansys Help [24].



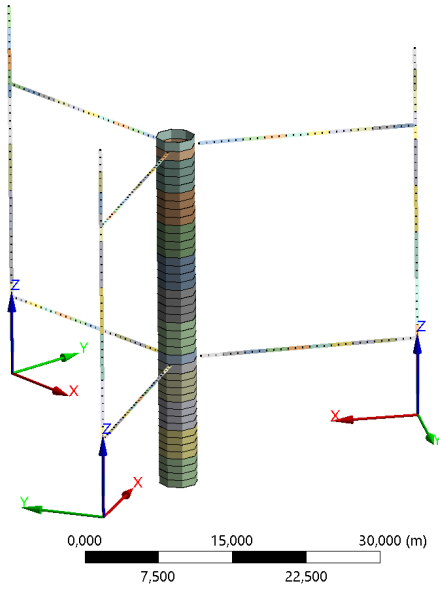


**Figure 5.8:** Local coordinate systems in which the aerodynamic forces are applied.

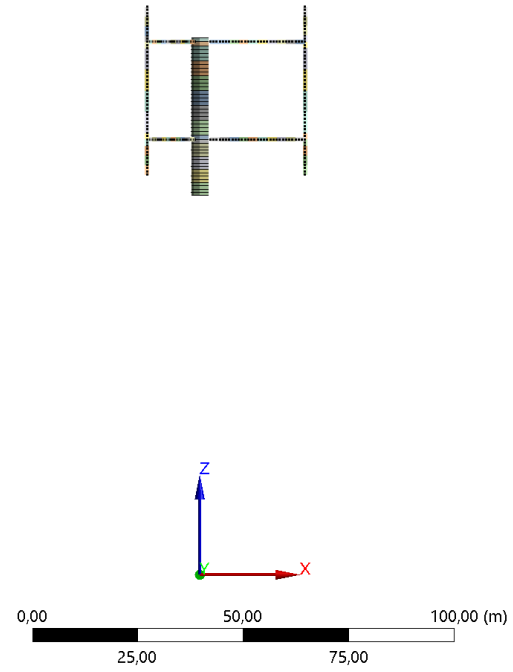


**Figure 5.9:** The global coordinate system having its origin at the bottom of the spar buoy (not shown).

property. Furthermore, element results, such as strains, are defined in the local element coordinate systems defined according to the Cross-Section Alignment.

The aerodynamic loads were applied in local coordinate systems created in Mechanical. These coordinate systems were aligned with the blade element coordinate systems and are shown in Figure 5.8.

The origin of the global coordinate system is set at the bottom of the spar buoy with the positive z-axis pointing upwards along the tower, which is shown in Figure 5.9.

### 5.5.4 Struts

The upper and lower struts were parameterized and optimized individually. The struts were modeled with quadratic BEAM188 elements and divided evenly long sections, which is shown in Figure 5.10. The initial vertical position of the struts was defined from the blade length and an input parameter, stating the initial vertical position in percent of the blade length. The properties and the parameters of the cross-sections were defined as described in Section 5.4.1.

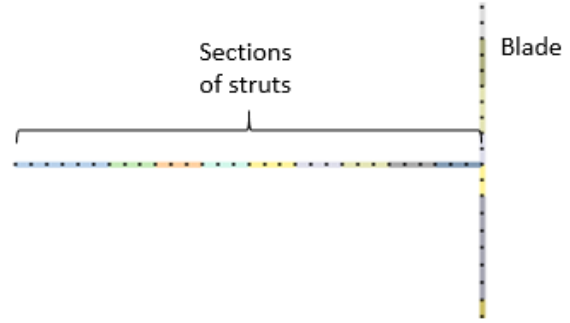


**Figure 5.10:** One strut divided in sections (colour scheme) and elements (dots).

### 5.5.5 Blades

Quadratic BEAM188 elements were used to model the blades. The blades were divided into sections as shown in Figure 5.11. The length of the sections closest to the strut connections was dependent on the initial blade length and kept constant during the optimization. This was done since the highest strains were assumed to occur there. The other parts of the blades (the bottom, middle, and top parts) were evenly divided into the desired number of sections. The properties and the parameters of the cross-sections were defined as described in Section 5.5.1. A toe out of 2 deg was used for the blades. All blades were modeled identically.

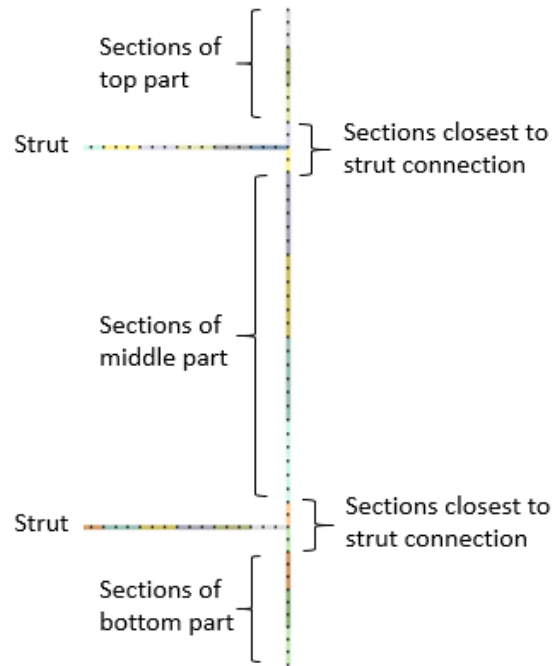


**Figure 5.11:** One blade divided in sections (colour scheme) and elements (dots).

### 5.5.6 Tower

The tower was modeled with quadratic BEAM188 elements and circular tube cross-sections. The cross-section properties were hence defined from the inner and outer radius, which were defined according to Section 5.4.3. The length of the sections closest to the strut connections was dependent on the initial diameter of the tower and kept constant during the optimization. The rest of the tower (the bottom and the top part) was evenly divided into the desired number of sections.

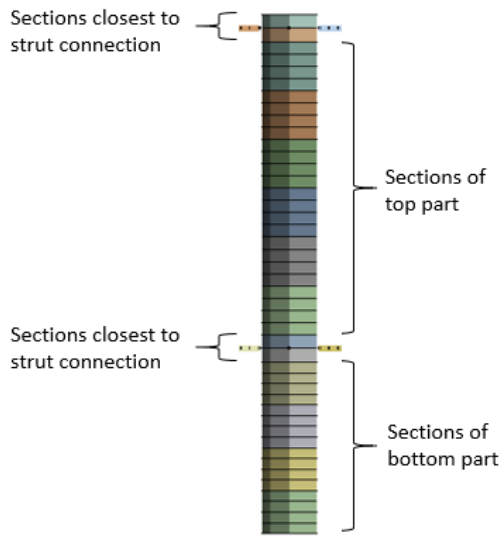


**Figure 5.12:** The tower divided in sections (colour scheme) and elements (lines).

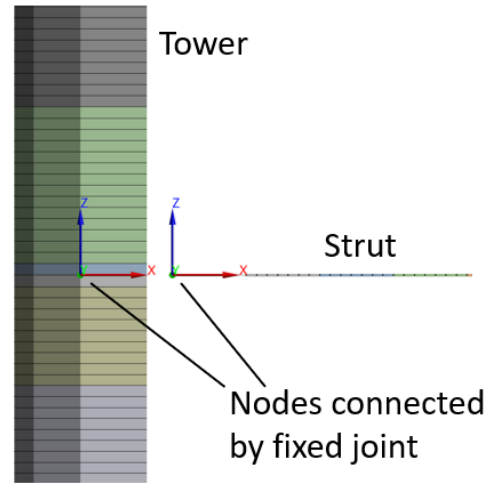


**Figure 5.13:** Illustration of a connection between the tower and one of the struts.

### 5.5.7 Connections

The connections between the tower and the struts are modeled with fixed joints in Ansys, which constrain all the degrees of freedom. The connections are modeled with a length corresponding to the radial length of the hubs. One of the connections is shown in Figure 5.13.

There is no connection element in Ansys that allow for different stiffnesses in different rotational directions and also parameterize the stiffnesses. As a workaround, 1 mm long beam elements were used to model connections with different rotational stiffnesses. These elements were used in the connections between the struts and the blades. The ends of the beam elements were connected with the struts and blades by fixed joints. The only purpose of the elements were to be able to change the rotational stiffness of the element, and hence the rotation and moment transferred between the blades and the struts. No stresses or strains were evaluated in these elements. Validation tests were conducted in Ansys to ensure the desired behaviour of the beam element. Tests were also performed to calibrate the beam properties to correspond to fixed and pinned connections.

### 5.5.8 Additional mass

Additional mass is added to model the mass of winglets, connections, hubs, platforms, stairs and so on. The winglets are positioned at the ends of the blades. The winglets are non-structural, hence they were modeled as point masses. To determine how their masses vary with the chord length, the area of the winglets were assumed to vary as the half of a sphere,  $A \propto r^2$ . Assuming constant NACA profile ( $c \propto t$ ) gives:

$$m_w = m_{w,ini} \frac{c^2}{c_{ini}^2} \quad (5.16)$$

The design, and hence the mass, of the connections will vary as the design of the rotor change. How it will change is however hard to estimate. Investigations, aiming to scale the masses with the reaction loads in the connections were made during the project. Due to the multitude of loads and plenty of parameters affecting the reaction forces, estimating the reaction loads without solving the FE problem was considered to be either too complex or too inaccurate. The need for solving the problem to determine the masses would however lead to an iterative solution process and hence significantly increase the computational time. Hence, constant mass of the connections were assumed for each concept.

The mass of other parts as hubs, platforms and stairs, were modeled by an increase of the tower density. This is a simplification based on the assumption that an increase in tower diameter will lead to for example larger hubs and platforms and an increase in tower height will lead to for example more platforms and longer stairs. The density was calculated as:

$$\rho_{tower} = \rho_{material} + \frac{m_{add}}{V_{tower,ini}} \quad (5.17)$$

where  $\rho_{material}$  is the density of the tower material,  $V_{tower,initial}$  is the initial material volume of the tower, and  $m_{add}$  is the initial additional mass of hubs, platforms, stairs, etc, all based on S2X estimations.

### 5.5.9 Mesh

An element size of approximately 1 m was used in the whole model. As mentioned in Section 1.2, the aim of the project was to give a first indication of the suitability of a concept, rather than calculate exact results. Hence, element size of 1 m was considered accurate enough.

## 5.6 Optimization flow

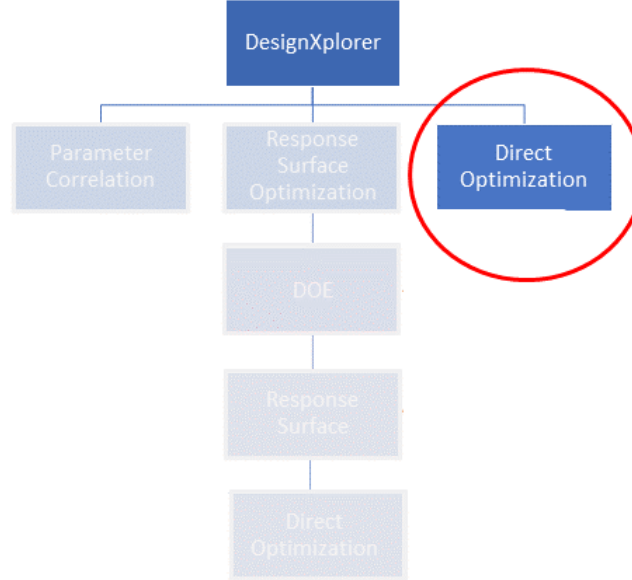


**Figure 5.14:** Outline of the DesignXplorer parametric optimization tools [24]. Only direct optimization was used out of all methods tried, as illustrated by the red circle.

As stated in Section 2.3, the three used tools in Ansys for this type of optimization are Parameter Correlation, Response Surface Optimization, and Direct Optimization. In this project, all were tested. Parameter Correlation, as well as Response Surface Optimization, was disregarded and finally, Direct Optimization was chosen as the tool to use, as visualized in Figure 5.14.

Parameter Correlation was initially tested with the aim to limit the design variables for the optimization while still maintaining an accurate model. The focus was on the struts and the blade as these ideally should be split into several sections that could have different properties to fully model these parts correctly. The idea was to use Parameter Correlation to see how different sections of the struts and the blade affected the first eigenfrequency and the strains. From this, one could then try to find a correlation between the sections and utilize this to rewrite the sections design variables,  $CS_{\text{strut},j,i}$ , as formulas all dependent on the first section's  $CS_{\text{strut},j,i}$ . Here  $j$  is the specific section of the strut while  $i$  indicates strut one or two. However, two things made this impossible. First, it was unclear whether Parameter Correlation can produce reasonable results with large amounts of design variables, as the results achieved during testing were uneven and varied. Secondly, the results showed no clear indication of a correlation between the sections that could be utilized to narrow

it down to one design variable.

Surface optimization was tested with the aim to achieve an optimization result in a shorter time span than with direct optimization. This also seemed like the most developed approach in Ansys. One DOE method, Central Composite Design, was tested together with two Response Surface Algorithms; the Genetic Aggregation and the full 2nd-order Polynomials. However, the Genetic Aggregation algorithm took too long time to generate and caused the program to slow down to the point where it was difficult to analyse the results. The 2nd-order Polynomials was quicker and easier to work with but did not achieve satisfactory results, even after refinements. Instead of testing further response surfaces, it was decided to focus on direct optimization.

Two optimization algorithms were initially tested within the Direct Optimization environment: AMO and MOGA. These were chosen as they are genetic algorithms with a focus on finding a global optimum while examining a large part of the design space. In Ansys, the MOGA is the more thorough method of investigating more design points, while the AMO is slightly less costly in terms of computer time. Several optimizations were run to determine which algorithm that obtained the best result, ending in the MOGA being chosen as this was the algorithm that converged most times and produced reliable results. The algorithm settings were set according to the automatic run-time index 9 in ANSYS [24].

Finally, four initial MOGA optimizations, two for the 1 MW design and two for the 10 MW design, with 8 design variables were run. For both 1 and 10 MW, the rotor was optimized separately with a pinned and fixed connection. While the initial plan was to include further design variables, it was decided to limit the optimization initially so as to not utilize too many design variables. Although it would theoretically be possible to utilize a larger amount of variables in the design in Ansys, it was not possible due to the time limitations of the project. Each optimization took around 40-70 hours to complete. As mentioned in 4 each optimization should then be further analysed based on the results obtained to be able to draw reasonable conclusions. In this project, one further MOGA optimization was run for each result, but with certain design variables set as fixed depending on the previous optimization. For the two runs for the 1 MW, the further analysis also included a manual test where the struts were divided into three sections and the design variables of the cross-sections changed according to the strain results from the earlier optimization. To be able to compare the final results between the fixed and pinned rotors, the further optimizations were kept the same between the two 1 MW and the two 10 MW concepts. All optimizations are listed below:

- **1 MW fixed, design 1:** The S2X design SeaTwirl currently utilizes. This was optimized for Radius, attachment points for the struts and cross-sections for struts, and blades.
- **1 MW fixed, design 2:** Optimization was run further on the cross-section properties for the struts and blade.

- **1 MW fixed, design 3:** A manual test with different parameters for different sections for each strut was made.
- **1 MW pinned, design 1:** The S2X design SeaTwirl currently utilizes but with a pinned connection between strut and tower. This was optimized for Radius, attachment points for the struts, and cross-sections for struts and blades.
- **1 MW pinned, design 2:** The same optimization as for 1 MW fixed, design 2 to get an accurate comparison.
- **1 MW pinned, design 3:** The same manual test as for 1 MW fixed, design 3 to get an accurate comparison.
- **10 MW fixed, design 1:** The upscaled version of the S2X design SeaTwirl currently utilizes. Same design variables as the 1 MW optimization.
- **10 MW fixed, design 2:** Only the attachment points were optimized.
- **10 MW pinned, design 1:** The upscaled version of the S2X design SeaTwirl currently utilizes but with a pinned connection between strut and tower. Same design variables as the 1 MW optimization.
- **10 MW pinned, design 2:** The same as for 10 MW fixed, design 2 to get an accurate comparison.





# 6

## H-rotor designs

This section contains the fourth step of the method described in Chapter 4 for the H-rotor design. The most relevant inputs for the FE-modelling and the optimization are listed here. After, the results from the optimizations are presented.

### 6.1 Initial designs

The full initial design for the rotor can be seen in Figure 6.1 and 6.2. While the most relevant inputs are presented here, further inputs can be found in Appendix B.

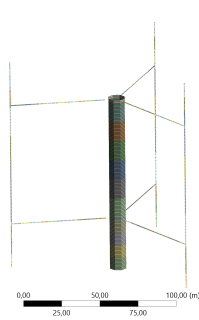


**Figure 6.1:** The initial design of the rotor, isometric view.

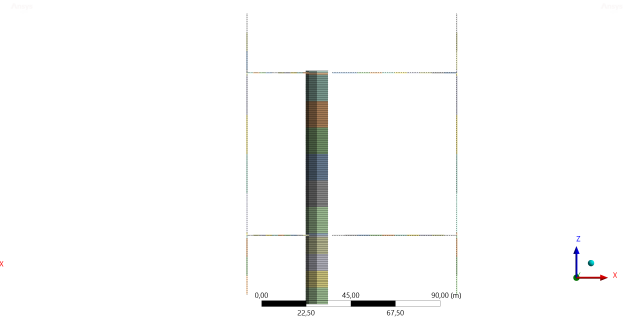


**Figure 6.2:** The initial design of the turbine, blade view.

### 6.1.1 1 MW

The design variable values and limits for the first optimization for the 1 MW rotor design are shown in Table 6.1. The design variables for further optimization and manual tests will be presented in Section 6.2.

Part	Variable name	Initial value	Lower limit	Upper limit
Full rotor	$R$ [m]	25	16	31
Strut	$AP_{\text{strut},1,p}$ [-]	0.5	0	1
Strut	$I_{\text{strut},1,p}$ [-]	0.5	0	1
Strut	$AP_{\text{strut},2,p}$ [-]	0.5	0	1
Strut	$I_{\text{strut},2,p}$ [-]	0.5	0	1
Strut	$CS_{\text{strut},1}$ [-]	1	0.1	2
Strut	$CS_{\text{strut},2}$ [-]	1	0.1	2
Blade	$CS_{\text{blade}}$ [-]	1	0.1	2

**Table 6.1:** Design variables used in the first 1 MW optimizations.

Furthermore, the constraints for strain and eigenfrequency were set. For the blades and the struts, the maximum absolute strain was not allowed to concede 0.2%. The first eigenfrequency had to be 10% larger than the 3P frequency.

Further inputs for the optimization can be found in Appendix B. Table B.6 and B.5 shows the fixed parameters and parameters based on relationships to the design variables for the initial optimization. These were not changed for other optimizations. The fixed parameters were defined from the current values of the S2X, as were the initial values for the design variables. The upper and lower limit of the radius of the rotor were as based on studies of optimal rotor aspect ratio discussed in Section 2.1.1. The remaining parameter values were based on formulas of design variables and fixed parameters, as described in Table B.5. The values for the formula parameters were all dependent on one or more design variables.

The inputs for the economic analysis are shown in Table B.1 in Appendix B. These numbers were based on the current VCOG, mass, CoB, and costs of the S2X. The costs were stated as the full cost for each part. The inputs for the fatigue analysis are shown in Table B.7 and B.3. The first table shows the damage curve, DFF, and lifespan used, as also stated in Section 5.3.3. The second table shows the inputs and initial thickness required to reach a total damage of less than 0.5 according to Equation (2.15). The total damage shown here adds up to 0.413. In Ansys, the values for the wind speed of 12 m/s were used as input. The scale factors for the load analysis are shown in Table B.4 in Appendix B. These were used to scale the forces as described in Section 5.5.2.

### 6.1.2 10 MW

The design variables for the initial 10 MW optimization are shown in Table 6.2.

Part	Variable name	Initial value	Lower limit	Upper limit
Full rotor	$R$ [m]	70.5	50.5	99.5
Strut	$AP_{\text{strut},1,p}$ [-]	0.5	0	1
Strut	$I_{\text{strut},1,p}$ [-]	0.5	0	1
Strut	$AP_{\text{strut},2,p}$ [-]	0.5	0	1
Strut	$I_{\text{strut},2,p}$ [-]	0.5	0	1
Strut	$CS_{\text{strut},1}$ [-]	1	0.1	2
Strut	$CS_{\text{strut},2}$ [-]	1	0.1	2
Blade	$CS_{\text{blade}}$ [-]	1	0.1	2

**Table 6.2:** Design variables used in the 10 MW optimizations.

The constraints for the 10 MW were set to the same as for the 1 MW, 0.2% for the absolute maximum strain and a first natural eigenfrequency of at least 10% over the 3P frequency. However, a strictly up-scaled version of the 1 MW rotor did not fulfill the strain criteria in the initial design for 10 MW. Therefore, the chord length was analytically estimated so that the max strain of the initial design did not exceed 0.15%.

The inputs for the economic analysis, the scale factors for the loads, and the parameters that were decided by relationships to the design variables were the same for the 10 MW rotor as for the 1 MW rotor. Regarding the inputs for the fatigue analysis; the load cases and  $C_d$  were the same. Further parameters for the fatigue analysis as well as the inputs for the fixed parameters are shown in Table B.7, B.8 and B.9 in Appendix B. The total damage value,  $D$ , for the fatigue reached 0.5.

## 6.2 Optimized designs

For each optimization, three candidate points were found. The first candidate point showcases the model with the lowest goal function value and is presented in this section. The goal function,  $G$ , value is as described in Section 5.2 and has no unit. The data from the two secondary candidate points are also written for comparison, while the images of these can be found in Appendix A.

### 6.2.1 1 MW

The optimization 1 MW fixed, design 1 resulted in a best candidate according to Figure 6.3. The values of the design variables, constraints and goal function are shown in Table 6.3 together with the values for the other two optimized candidate points. For the second design of the same concept, only the cross sections were varied, see Section 5.6, and hence the candidates had the same geometry as in Figure 6.3. The values of 1 MW fixed, design 2 are shown in Table 6.4 while the values of 1 MW fixed, design 3 are shown in Table 6.5. From Table 6.3, 6.4, and 6.5 it can be seen that the the goal function has decreased significantly for all designs, with the third design reaching the lowest value.

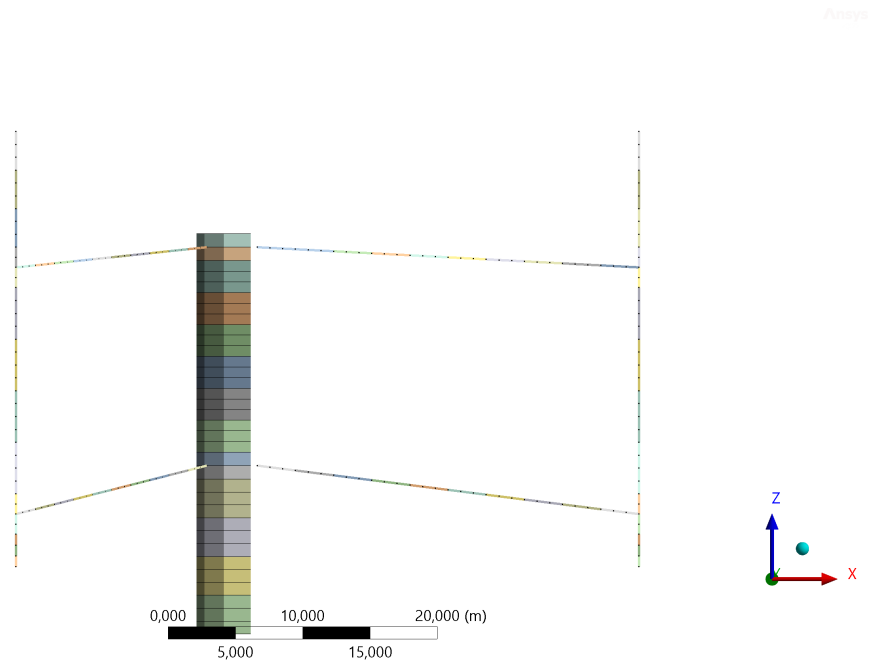


**Figure 6.3:** Candidate point 1 from optimization 1 MW fixed, design 1 and design 2.

Variable	Initial value	Lower limit	Upper limit	C. Point 1	C. Point 2	C. Point 3
$R$ [m]	25	16	31	30.9	30.8	30.8
$AP_{\text{strut},1,p}$ [-]	0.5	0	1	0.62	0.76	0.050
$I_{\text{strut},1,p}$ [-]	0.5	0	1	0.14	0.14	0.14
$AP_{\text{strut},2,p}$ [-]	0.5	0	1	0.20	0.18	0.18
$I_{\text{strut},2,p}$ [-]	0.5	0	1	0.35	0.32	0.30
$CS_{\text{strut},1}$ [-]	1	0.1	2	0.23	0.33	0.29
$CS_{\text{strut},2}$ [-]	1	0.1	2	0.42	0.42	0.45
$CS_{\text{blade}}$ [-]	1	0.1	2	0.68	0.62	0.60
$f_1/f_{3P}$ [-]	1.73	1.1	-	1.60	1.72	1.66
$ \epsilon _{\text{max}}$ [%]	0.13	-	0.20	0.20	0.19	0.19
$G$ [-]	17720	-	-	8625	8687	8693

**Table 6.3:** Design variables, constraints, and the goal function for candidate points from optimization 1 MW fixed, design 1.

Variable	Initial value	Lower limit	Upper limit	C. Point 1	C. Point 2	C. Point 3
$CS_{\text{strut},1}$ [-]	0.23	0.1	0.5	0.22	0.23	0.23
$CS_{\text{strut},2}$ [-]	0.42	0.1	0.7	0.42	0.42	0.42
$CS_{\text{blade}}$ [-]	0.68	0.1	0.9	0.56	0.56	0.56
$f_1/f_{3P}$ [-]	1.6	1.1	-	1.64	1.65	1.65
$ \epsilon _{\text{max}}$ [%]	0.20	-	0.20	0.20	0.20	0.20
$G$ [-]	8625	-	-	8310	8322	8335

**Table 6.4:** Design variables, constraints, and the goal function for candidate points from optimization 1 MW fixed, design 2.

Variable	Initial value	New value
$CS_{\text{strut},1,1-3,p}$ [-]	0.22	0.22
$CS_{\text{strut},1,4,p}$ [-]	0.22	0.17
$CS_{\text{strut},1,1-5-10,p}$ [-]	0.22	0.15
$CS_{\text{strut},2,1-3,p}$ [-]	0.42	0.42
$CS_{\text{strut},2,4-6,p}$ [-]	0.42	0.32
$CS_{\text{strut},2,7-10,p}$ [-]	0.42	0.21
$f_1/f_{3P}$ [-]	1.64	1.60
$ \epsilon _{\text{max}}$ [%]	0.20	0.20
$G$	8310	7992

**Table 6.5:** Old and updated design variables, constraints, and the goal function for 1 MW fixed, design 3.

The first candidate point of the optimized 1 MW pinned, design 1 can be seen in Figure 6.4. In Table 6.6, the values for all candidate points from the same concept

are shown. As described in Section 5.6, 1 MW model pinned, design 2 was only optimized with regards to the cross-section properties, compared to design 1. The geometry is therefore the same as for design 1 in Figure 6.4. The values for all candidate points of 1 MW pinned, design 2 are shown in Table 6.7. From the manual test in 1 MW pinned, design 3, the values shown in Table 6.8 were obtained.

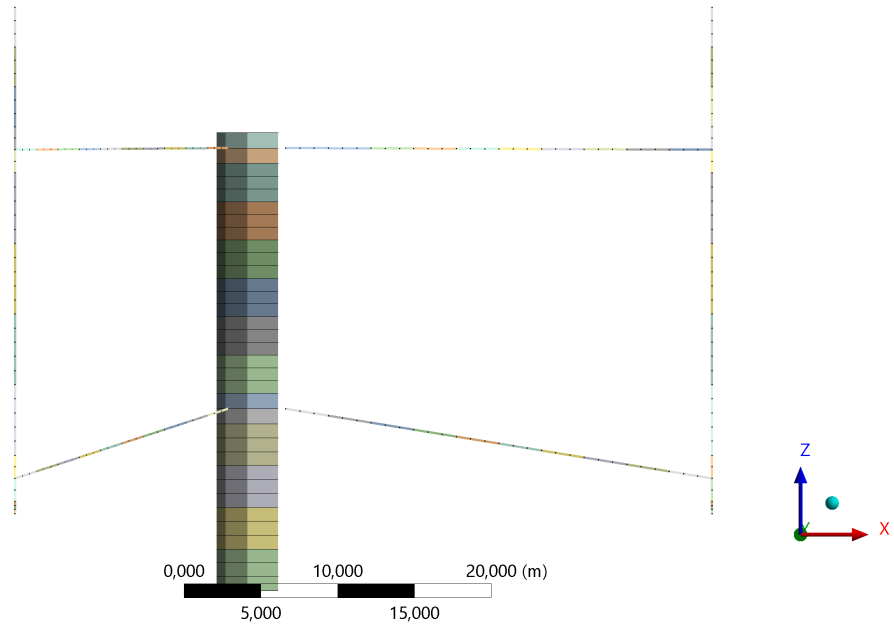


**Figure 6.4:** Candidate point 1 from optimization 1 MW pinned, design 1 and design 2.

Variable	Initial value	Lower limit	Upper limit	C. Point 1	C. Point 2	C. Point 3
$R$ [m]	25	16	31	30.2	30.1	30.1
$AP_{\text{strut},1,p}$ [-]	0.5	0	1	0.49	0.46	0.46
$I_{\text{strut},1,p}$ [-]	0.5	0	1	0.036	0.79	0.20
$AP_{\text{strut},2,p}$ [-]	0.5	0	1	0.13	0.10	0.11
$I_{\text{strut},2,p}$ [-]	0.5	0	1	0.49	0.36	0.34
$CS_{\text{strut},1}$ [-]	1	0.1	2	0.40	0.45	0.44
$CS_{\text{strut},2}$ [-]	1	0.1	2	0.52	0.47	0.52
$CS_{\text{blade}}$ [-]	1	0.1	2	0.60	0.61	0.61
$f_1/f_{3P}$ [-]	1.38	1.1	-	1.30	1.29	1.32
$ \epsilon _{\text{max}}$ [%]	0.081	-	0.20	0.15	0.19	0.20
$G$ [-]	17720	-	-	9203	9240	9336

**Table 6.6:** Design variables, constraints, and the goal function for candidate points from optimization 1 MW pinned, design 1.

Variable	Initial value	Lower limit	Upper limit	C. Point 1	C. Point 2	C. Point 3
$CS_{\text{strut},1}$ [-]	0.40	0.1	0.5	0.22	0.22	0.22
$CS_{\text{strut},2}$ [-]	0.52	0.1	0.6	0.55	0.55	0.55
$CS_{\text{blade}}$ [-]	0.6	0.1	0.7	0.45	0.45	0.45
$f_1/f_{3P}$ [-]	1.30	1.1	-	1.30	1.31	1.31
$ \epsilon _{\text{max}}$ [%]	0.15	-	0.20	0.20	0.20	0.20
$G$ [-]	9203	-	-	8522	8525	8527

**Table 6.7:** Design variables, constraints, and the goal function for candidate points from optimization 1 MW pinned, design 2.

Variable	Old values	New values
$CS_{\text{strut},1,1-3}$ [-]	0.22	0.22
$CS_{\text{strut},1,4-5}$ [-]	0.22	0.17
$CS_{\text{strut},1,6-10}$ [-]	0.22	0.11
$CS_{\text{strut},2,1}$ [-]	0.55	0.55
$CS_{\text{strut},2,2-4}$ [-]	0.55	0.41
$CS_{\text{strut},2,5-10}$ [-]	0.55	0.28
$f_1/f_{3P}$ [-]	1.30	1.19
$ \epsilon _{\text{max}}$ [%]	0.20	0.20
$G$ [-]	8522	7978

**Table 6.8:** Old and updated design variables, constraints, and the goal function for 1 MW pinned, design 3.

### 6.2.2 10 MW

The best candidate from optimization 10 MW fixed, design 1 is shown in Figure 6.5. The values of the design variables, constraints and goal function are shown in Table 6.9 together with the values for the other two optimized candidate points. The second design of the same concept, where the attachment points were optimized according to Section 5.6, resulted in an optimal geometry shown in Figure 6.6. The values of 10 MW fixed, design 2 are shown

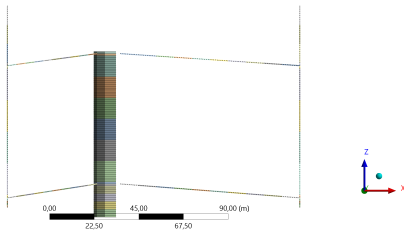


**Figure 6.5:** Candidate point 1 from optimization 10 MW fixed, design 1.

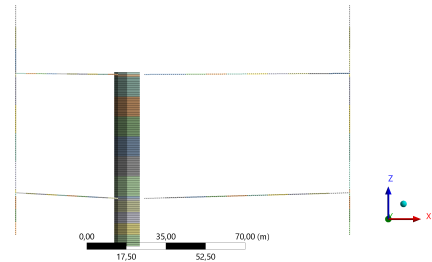


**Figure 6.6:** Candidate point 1 from optimization 10 MW fixed, design 2.

Variable	Initial value	Lower limit	Upper limit	C. Point 1	C. Point 2	C. Point 3
$R$ [m]	70.5	50.5	99.5	98.3	98.0	95.8
$AP_{\text{strut},1,p}$ [-]	0.5	0	1	0.00	0.41	0.47
$I_{\text{strut},1,p}$ [-]	0.5	0	1	0.28	0.34	0.34
$AP_{\text{strut},2,p}$ [-]	0.5	0	1	0.36	0.35	0.36
$I_{\text{strut},2,p}$ [-]	0.5	0	1	0.31	0.15	0.15
$CS_{\text{strut},1}$ [-]	1	0.1	2	0.32	0.32	0.32
$CS_{\text{strut},2}$ [-]	1	0.1	2	0.30	0.30	0.27
$AP_{\text{blade}}$ [-]	1	0.1	2	0.60	0.60	0.60
$f_1/f_{3P}$ [-]	1.77	1.1	-	2.43	2.62	2.52
$ \epsilon _{\text{max}}$ [%]	0.17	-	0.20	0.20	0.19	0.20
$G$ [-]	603200	-	-	202500	203100	211400

**Table 6.9:** Design variables, constraints, and the goal function for candidate points from optimization 10 MW fixed, design 1.

Variable	Initial value	Lower limit	Upper limit	C. Point 1	C. Point 2	C. Point 3
$AP_{\text{strut},1,p}$ [-]	0.00	0	1	0.23	0.23	0.47
$I_{\text{strut},1,p}$ [-]	0.28	0	1	0.58	0.58	0.58
$AP_{\text{strut},2,p}$ [-]	0.36	0	1	0.015	0.015	0.015
$I_{\text{strut},2,p}$ [-]	0.31	1	1	0.51	0.47	0.51
$f_1/f_{3P}$ [-]	2.43	1.1	-	2.56	2.59	2.58
$ \epsilon _{\text{max}}$ [%]	0.20	-	0.20	0.19	0.19	0.18
$G$ [-]	202500	-	-	193200	193200	193200

**Table 6.10:** Design variables, constraints, and the goal function for candidate points from optimization 10 MW fixed, design 2.

With a pinned connection between the struts and blades, the best candidate point for optimization 10 MW pinned, design 1 is shown in Figure 6.7. The values of the design variables, constraints and goal function for the three candidate points are shown in Table 6.11. The optimized geometry of 10 MW pinned, design 2 according to 5.6 is shown in Figure 6.8 and the values of all candidate points of 10 MW pinned, design 2 are shown in Table 6.12.

Comparing the values for fixed versus pinned connections between the struts and the blades, as listed in Table 6.9-6.12, it can be seen that the goal function reaches a lower value for when pinned connections are used.



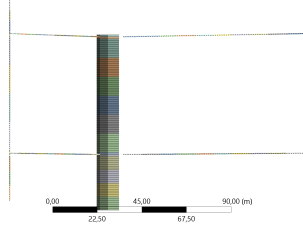


**Figure 6.7:** Candidate point 1 from optimization 10 MW pinned, design 1.

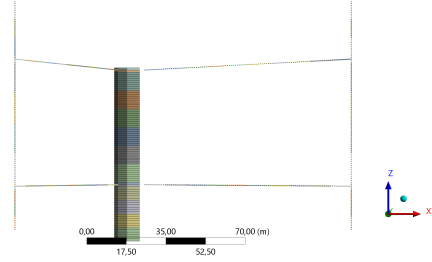


**Figure 6.8:** Candidate point 1 from optimization 10 MW pinned, design 2.

Variable	Initial value	Lower limit	Upper limit	C. Point 1	C. Point 2	C. Point 3
$R$ [m]	70.5	50.5	99.5	99.0	97.9	94.3
$AP_{\text{strut},1,p}$ [-]	0.5	0	1	0.60	0.61	0.54
$I_{\text{strut},1,p}$ [-]	0.5	0	1	0.52	0.50	0.50
$AP_{\text{strut},2,p}$	0.5	0	1	0.65	0.65	0.32
$I_{\text{strut},2,p}$	0.5	0	1	0.55	0.54	0.55
$CS_{\text{strut},1}$	1	0.1	2	0.30	0.32	0.32
$CS_{\text{strut},2}$ [-]	1	0.1	2	0.27	0.26	0.25
$CS_{\text{blade}}$ [-]	1	0.1	2	0.31	0.28	0.29
$f_1/f_{3P}$ [-]	1.60	1.1	-	2.08	2.15	2.07
$ \epsilon _{\max}$ [%]	0.15	-	0.20	0.18	0.18	0.17
$G$ [-]	603200	-	-	182700	184200	188600

**Table 6.11:** Design variables, constraints, and the goal function for candidate points from optimization 10 MW pinned, design 1.

Variable	Initial value	Lower limit	Upper limit	C. Point 1	C. Point 2	C. Point 3
$AP_{\text{strut},1,p}$ [-]	0.60	0	0.7	0.43	0.30	0.43
$I_{\text{strut},1,p}$ [-]	0.52	0	0.6	0.48	0.42	0.49
$AP_{\text{strut},2,p}$ [-]	0.65	0	0.7	0.020	0.30	0.30
$I_{\text{strut},2,p}$ [-]	0.55	0	0.7	0.65	0.48	0.65
$f_1/f_{3P}$ [-]	2.08	1.1	-	2.08	2.08	2.08
$ \epsilon _{\max}$ [%]	0.17	-	0.20	0.19	0.20	0.17
$G$ [-]	182700	-	-	165800	173200	173300

**Table 6.12:** Design variables, constraints, and the goal function for candidate points from optimization 10 MW pinned, design 2.



# 7

## Discussion

This section includes both a discussion of the developed method and the obtained optimization results of the studied concepts. This conducts the final step of the method from Section 4, analysing and interpreting the results of the optimization.

### 7.1 Method development

The method developed in this thesis should be possible to utilize as a concept evaluation tool at an early stage of the product development process described in Section 1.1.2. As stated in Section 4, this means that the method should fairly and efficiently evaluate concepts of which there are little known. In the scope of this project, the constructed method was tested on a simplified H-rotor model, resulting in an indication of optimal design. When there is little knowledge about a product, it is necessary to utilize simplifications within concept evaluation, as reliable information regarding each design is not readily available and would be time-consuming to investigate. It is therefore natural that this evaluation concludes in indications, which can then be utilized to move the development process forward. In the aspect of suitability for early development, this method therefore reaches the aim described in Section 1.2.

It is further important to discuss whether the results found through the method were reliable. For example, several assumptions regarding the relationships between parameters were made to limit the amount of design variables. The found optimal designs were therefore heavily influenced by how these relationships were set. While this could be further investigated, it is reasonable to believe that the designs found are reliable indications of an optimal rotor, as the relationships were based on analytical calculations and common practices within the field of FVAWTs. The results are also further analysed in Section 7.2, and indicates that the method can produce valuable insights for further development of FVAWT. Furthermore, the method has proved to be adaptable for different types of H-rotor concepts, and it is believed that it can be further utilized for other FVAWT designs. Even if this was not tested within the scope of this project, no results indicating the opposite were found.

Some parts of this method could be approached differently. In this study, the initial optimizations included design variables of all rotor parts. The optimizations were then reduced to focus on fewer design variables, based on the previous results. It

would be possible to do vice versa and instead start with less design variables. However, it was decided to not use this approach for several reasons. For example, optimizing on few design variables initially, and then gradually expand the scope by locking the design variables already optimized on, might accidentally lead to sub-optimizations where the global optima would not be found. Furthermore, starting with an initial optimization of the full rotor gave insight and information that could be used to focus on specific design variables or parts of the structure. What parts to focus on was not clear before these optimizations were conducted.

During the scope of the project, different optimization approaches were tested as stated in Section 5.6. For example, a parameter correlation and DOE study were investigated, but did not achieve adequate results. However, it might be possible to use similar approaches in another tool or if other constraints or design variables are prioritized. Furthermore, it is recommended to use a combination of optimizations and manual tests in the method. A manual test can be a quick way to test constraints and results without a time consuming optimization.

Finally, the method has some limitations. To begin with, it will not be possible to use the method if the required prerequisites are not available. Hence, it is difficult to utilize the method on very novel concepts where, for example, no data or information about the aerodynamic loads are available. Furthermore, it is not certain that the optimal rotor has been found due to uncertainties always present in advanced optimization procedures, for example, there is a possibility that a global optima has not been found. The used optimization algorithm, MOGA, gives clear indications regarding some design variables, but did not converge for every optimization. However, with further optimizations and studies, the method still obtained results which strongly indicates that the found optima was close to the global optima.

Furthermore, large parts of the method can be utilized without utilizing optimization. For example, different designs could be tested manually, similar to what was done with design 3 of the two 1 MW optimizations, and produce interesting results without completing a full optimization. However, as it is not certain that the initial design of a concept is close to the optimal design, utilizing optimization contributes to fair evaluation between different concepts. By utilizing optimization, the best design of each concepts are compared to each other.

## 7.2 Optimization results

To evaluate the results from the optimizations, the optimized values for each design variable will be analysed in this section, as well as their effect on the goal function and constraints regarding strain and eigenfrequency.

To begin with, the radius of the rotor,  $R$ , did always go towards its upper limit. Regarding the goal function,  $R$  affects the mass of the struts, blade, and tower. A larger radius results in longer struts but shorter blades. The assumption is that the chord length scale linear with  $R$  leads to lower mass per stiffness when  $R$  increases.

A larger radius also implies a thinner tower due to a lower bending moment in the fatigue analysis. These effects must be considered together with the different material costs for the different parts, where especially the tower material is considerably cheaper than the strut and blade materials. Altogether, the results show that an increase in  $R$  decreases the goal function for all studied concepts. It is here important to notice that no aerodynamic properties are included in the optimization. For example, longer and thicker struts should cause more drag and hence possible greater loss in efficiency,  $C_p$ . On the other hand, due to constant  $\lambda$ , an increased radius implies a lower rotational velocity, which should give less drag and hence be advantageous for  $C_p$ .

Furthermore, increasing the radius was not restricted by any constraint. An early hypothesis was that the eigenfrequency criteria would limit a large radius, since a large radius would reduce the first eigenfrequency. However, the constraint regarding the eigenfrequency was only defined based on the 3P frequency, which was also reduced with larger  $R$ , and therefore this criterion did not limit the design variable.

The design variables for the cross-section of the struts and the blades were decreased in all optimizations without reaching their lower limit. To investigate this further, optimizations were performed on the 1 MW designs with only the struts and blade cross-section parameters as design variables. Even if this led to further reductions, especially on the blades, it was clear that the cross-section properties were limited by the strain criteria. Comparing the concepts with fixed and pinned connections between struts and blade, the blade cross-section variable was reaching a lower value when a pinned connection was used, while the cross-section variable of the upper strut reached a lower value with a fixed connection. This is reasonable since no moment can be transferred in a pinned connection.

Regarding the attachment point and inclination of the struts, the design variables varied between the candidate points of the optimizations. Often, no clear indication of an optimal attachment point between the struts and the tower, or the angle of the struts was found. This was further investigated in the second optimizations of the 10 MW rotors. By analysing these optimizations and previous runs, some explanations were found. To begin with, the attachment point for strut 1 alone did not have a great effect on the goal function or the active constraint regarding strain. Furthermore, the inclination of both struts did not affect the goal function majorly, but seemed to affect the strains in the blades. This is reasonable as the attachment point between the struts and the blade affect the section moments in the blade. Finally, the attachment point between strut two and the tower had a greater effect on the goal function as this point defined the height of the tower. However, this was not clear in the initial optimizations with eight variables. Reasons for this could be that these optimizations did not converge and that the attachment point affected the goal function relatively little compared to other design variables. Instead, in further optimizations with four variables, it was clear that this variable tended towards its lower limit. From these results, it was also assumed that the point alone had a low effect on the strain criteria, as long as the inclination of the strut gave a favorable

attachment position between the strut and blade.

As seen in the results in Section 6.2, the strain criteria was the only active criteria in all performed optimizations while the eigenfrequency criteria did not influence the optimized designs. One reason for the constraint not being active might be the constant cross-sections of the struts and blade used in the optimizations, which is highly simplified compared to the actual design of S2X. Therefore, a further study with struts divided into sections with different cross-sections was performed for the 1 MW designs by manual tests. While the frequency constraint did not become active in these tests, the constraint was lowered, especially for the pinned connection design. It is therefore feasible to believe that the frequency might be a limitation for the strut and blade design if these are further divided into separate sections. As discussed above, basing the constraint only on the 3P frequency was a further reason for the inactive frequency constraint.

Comparing the two different wind turbine sizes, 1 MW and 10 MW, considered in this project, the optimizations resulted in similar optimal designs. It should however be noted that for the 10 MW concept, the chord length could not be scaled linearly from the 1 MW concept. When it was, the strain constraint was not fulfilled even if the cross-section properties were increased by enlarging the thickness of the laminate. From FE simulations it was shown that the impact from the gravitational and the centrifugal forces was larger compared to the aerodynamical forces for the 10 MW wind turbine. Hence, increasing the stiffness through a larger thickness will also increase the mass, and subsequently the mass-dependent forces. Due to this kind of nonlinearities, it can be stated that an optimal design for one size cannot be scaled to obtain the optimal design of another size. In this project, this problem was solved by further lengthening the chord of the 10 MW concept to get a better stiffness-per-mass ratio. It should however be noted that this affects the solidity and hence probably also the aerodynamic performance, which was not investigated within this project.

Finally, for each concept, the goal function of the initial model was lowered by more than 50% after the optimizations. While this shows possibilities for great improvements to the design, it is not reasonable to believe that the total cost of the rotor of the S2X can be lowered by over 50%. A large number of assumptions regarding the costs were made to reduce the scope of the project and the H-rotor model used is a vastly simplified version of the S2X. For example, the production cost of the turbine might vary for different designs found in the optimization, and the rotor designs found in this study might not be optimal from this cost perspective. Further investigations at later stages of the design process should therefore be considered before a final conclusion regarding the cost reduction can be made.

# 8

## Conclusion

The project aimed to complete the following:

1. Construct a method for efficient evaluation of the rotor of an H-rotor VAWT at an early stage of product development.
2. Utilize this method on a 1 MW and 10 MW H-rotor to find indications regarding the optimal design.

Regarding the first aim, the constructed method has been described in Section 4 and further analysed in Section 7. In summary, it was concluded that the workflow is well suited for early evaluation of H-rotor concepts and that it likely can be applied to other concepts. Through the presented assumptions and relations, the number of design variables could be limited, enabling optimization on the structure. However, the method requires certain prerequisites that might not be available for novel concepts. Finally, it results in an indication of an optimal design, which is acceptable for an evaluation at this stage of the product development process as discussed in Section 7.

For the second aim, optimizations of a 1 MW and a 10 MW rotor were constructed, implemented, and analysed in Section 5 and 7. For both the 1 MW and the 10 MW rotor it can be concluded that, according to the method developed, a large rotor radius, and thereby short blades, was ideal. The angle and the attachment position of the struts did not show a large impact on the goal function, even if a lower attachment point of the upper struts, and hence a shorter tower, decreased the goal function. All optimizations decreased the initial design variable of the cross-section, something that should be further investigated. Furthermore, a pinned or a fixed connection between the struts and the blades did not have a major impact on the goal function for the 1 MW rotor while a pinned connection was advantageous for the 10 MW rotor. Finally, it is once again important to note that these results are indications of an optimal design, given the constraints and goal function used in this study, and that further analyses are needed.





# 9

## Future work

This study has presented and tested a method for evaluating and optimizing a FVAWT rotor. However, there are several aspects regarding the limitations and assumptions in this project that should be addressed in future work. Some of these can be summarized as:

- Further tests on the H-rotor concept
- Buckling analysis
- Investigation of other software
- Investigating a method for general load analysis
- Perform optimization on other concepts

Initially, there are certain aspects of the H-rotor design and the variables here considered that can be further investigated. For example, it would be interesting to focus more on the tower design and optimize directly on design variables for this part. It would also be relevant to redesign the tower as tapered, as it is in the current S2X design, and further analyse this result. For the struts and blade, it would be of interest to continue testing the cross-section properties, and investigate how these affect the frequency constraint and goal function. Furthermore, it would be of interest to investigate further design variables of the rotor. For example, different materials, number of struts and blades, or other power levels can be considered.

Another aspect that can be considered in future work is buckling of the rotor as this is an important design criterion. It has not been investigated in this project due to its complexity, but in future work, it would be desirable to implement this into the method as well. It would also be interesting to consider the buckling and fatigue of the struts and blades.

Furthermore, this project has utilized tools from Ansys Workbench, with only DesignXplorer being considered for optimization. Unfortunately, some issues regarding the software have emerged during the scope that might be easier to handle in other programs or tools. For example, it has been difficult to handle parameters within the program as it often became slow and demanding to work with during optimiza-

tion. Therefore, a recommended future work is to investigate other possible tools, such as ANSYS Optislang, Abaqus, Comsol, and Matlab.

As stated in Section 5.1, aerodynamic loads must be available in order to utilize the method. This can be limiting if a concept should be evaluated at a very early stage and studies of earlier concepts cannot be used. It would therefore be interesting to look at possibilities to perform basic load analyses as a part of the scope of the method.

Finally, the model should be further tested for other concepts such as a Darrius turbine or a V-rotor. This would test the flexibility of the model, and highlight possible issues when comparing vastly different designs. For example, constructing a goal function that fairly describes the cost of each model could be a major challenge as the production cost is highly relevant. This work would also give a broader idea of the ideal rotor design for a FVAWT.

# Bibliography

- [1] Global Wind Energy Council. *Global wind report 2021*. Jan. 2022. URL: <https://gwec.net/global-wind-report-2021/>.
- [2] International Energy Agency. *Renewables 2021 - analysis and forecast to 2026*. Dec. 2021. URL: <https://iea.blob.core.windows.net/assets/5ae32253-7409-4f9a-a91d-1493ffb9777a/Renewables2021-Analysisandforecastto2026.pdf>.
- [3] *What is the future of wind energy?* Apr. 2021. URL: <https://scienceexchange.caltech.edu/topics/sustainability/wind-energy-advantages-disadvantages>.
- [4] Laura Castro-Santos and Vicente Diaz-Casas. *Sensitivity analysis of floating offshore wind farms*. June 2015. URL: <https://www.sciencedirect.com/science/article/pii/S0196890415004793>.
- [5] M. Dolores Esteban et al. *Why offshore wind energy?* Aug. 2010. URL: <https://www.sciencedirect.com/science/article/abs/pii/S0960148110003332>.
- [6] *SeaTwirl Internal Document*. 2022.
- [7] Yan Li. *Straight-Bladed Vertical Axis Wind Turbines: History, Performance, and Applications*. 2019. URL: [https://www.researchgate.net/publication/n/331617997\\_Straight-Bladed\\_Vertical\\_Axis\\_Wind\\_Turbines\\_History\\_Performance\\_and\\_Applications](https://www.researchgate.net/publication/n/331617997_Straight-Bladed_Vertical_Axis_Wind_Turbines_History_Performance_and_Applications).
- [8] D. Todd Griffith et al. *Design studies for deep-water floating offshore vertical axis wind turbines.r*. Jan. 2018. URL: <https://www.semanticscholar.org/paper/Design-Studies-for-Deep-Water-Floating-Offshore-Griffith-Barone/cfa088bc0f5ebde48bdc8c09acd188f886f8b2d5>.
- [9] F. Ottermo and H. Bernhoff. *An upper size of vertical axis wind turbines*. Jan. 1970. URL: <https://www.semanticscholar.org/paper/An-upper-size-of-vertical-axis-wind-turbines-Ottermo-Bernhoff/2cdce761cd850202e8a4053c73bbcaf975c2466>.
- [10] F. González-Longatt, P. Wall, and V. Terzija. *Wake effect in wind farm performance: Steady-state and dynamic behavior*. Sept. 2011. URL: <https://www.sciencedirect.com/science/article/pii/S0960148111005155>.
- [11] Joachim Toftegaard Hansen, Mahak Mahak, and Iakovos Tzanakis. *Numerical modelling and optimization of vertical axis wind turbine pairs: A scale up approach*. Mar. 2021. URL: <https://www.sciencedirect.com/science/article/pii/S096014812100344X>.

- [12] Herbert J. Sutherland, Dale E. Berg, and Thomas D. Ashwill. *A Retrospective of VAWT Technology*. Jan. 2012. URL: <https://energy.sandia.gov/wp-content/gallery/uploads/SAND2012-0304.pdf>.
- [13] Karl T. Ulrich and Steven D. Eppinger. *Product design and development*. Sixth. McGraw Hill / Irwin, 2015.
- [14] Steven C. Wheelwright and Kim B. Clark. *Revolutionizing product development: Quantum leaps in speed, efficiency and quality*. Free Press/Simons amp; Schuster, 2011.
- [15] *SeaTwirl*. URL: <https://seatwirl.com/>.
- [16] Rupp Cariveau Mojtaba Ahmadi-Baloutaki and David S-K Ting. “Straight-bladed vertical axis wind turbine rotor design guide based on aerodynamic performance and loading analysis”. In: *Journal of Power and Energy* 228(7) (2014), pp. 742–759. DOI: 10.1177/0957650914538631.
- [17] M. Saqib Hameed and S. Kamran Afaq. “Design and analysis of a straight bladed vertical axis wind turbine blade using analytical and numerical techniques”. In: *Ocean Engineering* 57 (2013), pp. 248–255. ISSN: 0029-8018. DOI: <https://doi.org/10.1016/j.oceaneng.2012.09.007>. URL: <https://www.sciencedirect.com/science/article/pii/S0029801812003514>.
- [18] Charles L. Ladson et al. *Computer Program To Obtain Ordinates for NACA Airfoils*. 1996. URL: <https://www.pdas.com/refs/tm4741.pdf>.
- [19] Abdolrahim Rezaeiha, Hamid Montazeri, and Bert Blocken. “Towards optimal aerodynamic design of vertical axis wind turbines: Impact of solidity and number of blades”. In: *Energy* 165 (Sept. 2018), pp. 1129–1148. URL: <https://doi.org/10.1016/j.energy.2018.09.192>.
- [20] Sandra Eriksson, Hans Bernhoff, and Mats Leijon. “Evaluation of different turbine concepts for wind power”. In: *Renewable and Sustainable Energy Reviews* 12 (2008), pp. 1419–1434. DOI: 10.1016/j.rser.2006.05.017.
- [21] Det Norske Veritas and Risø National Laboratory Wind Energy Department. *Guidelines for Design of Wind Turbines*. Jydsk Centraltrykkeri, 2002. ISBN: 87-550-2870-5.
- [22] Magdi Ragheb and Adam M. Ragheb. *Wind Turbines Theory - The Betz Equation and Optimal Rotor Tip Speed Ratio, Fundamental and Advanced Topics in Wind Power, Dr. Rupp Cariveau (Ed.)* 2011. ISBN: 978-953-307-508-2.
- [23] Martin O.L.Hansen. “Basic Rotor Aerodynamics applied to Wind Turbines”. In: (1998). URL: <https://www.osti.gov/etdeweb/servlets/purl/618185>.
- [24] Ansys. *Ansys Help, Documentation, tutorials, and videos for Ansys products*. 2022.
- [25] Surya Patnaik and Dale Hopkins. *Strength of materials : A new unified theory for the 21st century*. Elsevier Science Technology, 2003.
- [26] Erasmo Carrera, Gaetano Giunta, and Marco Petrolo. *Beam Structures: Classical and Advanced Theories*. John Wiley Sons, 2011.
- [27] Yong Bai and Jin Wai-Liang. *Marine Structural Design*. Butterworth-Heinemann, 2016.
- [28] *Fatigue design of offshore steel structures*. DNV-RP-C203. DNV GL AS, 2016.

- [29] Panos Y. Papalambros and Douglass J. Wilde. *Principles of Optimal Design: Modeling and Computation*. Cambridge University Press, 2017.
- [30] Manny Uy and Jacqueline K. Telford. *Optimization by design of Experiment Techniques*. Apr. 2009. URL: <https://ieeexplore.ieee.org/document/4839625>.
- [31] Marta Carvalho et al. *Techniques adopted in integrating structural analysis with numerical optimization*. July 2006. URL: [https://www.researchgate.net/publication/262379877\\_TECHNIQUES\\_ADOPTED\\_IN\\_INTEGRATING\\_STRUCTURAL\\_ANALYSIS\\_WITH\\_NUMERICAL\\_OPTIMIZATION](https://www.researchgate.net/publication/262379877_TECHNIQUES_ADOPTED_IN_INTEGRATING_STRUCTURAL_ANALYSIS_WITH_NUMERICAL_OPTIMIZATION).
- [32] U.S. Energy Information Administration (EIA). *Annual Energy Outlook*. Mar. 2022. URL: <https://www.eia.gov/outlooks/aeo/>.
- [33] Magdi Ragheb. *Economics of wind power generation*. May 2017. URL: <https://experts.illinois.edu/en/publications/economics-of-wind-power-generation>.
- [34] Clara M. St Martin et al. *Wind turbine power production and annual energy production depend on atmospheric stability and turbulence*. 2016. URL: <https://www.nrel.gov/docs/fy17osti/66360.pdf>.
- [35] Jason Fernando. *Capital expenditure (CAPEX)*. Mar. 2022. URL: <https://www.investopedia.com/terms/c/capitalexpenditure.asp>.
- [36] Will Kenton. *What is an operating expense?* Mar. 2022. URL: [https://www.investopedia.com/terms/o/operating\\_expense.asp](https://www.investopedia.com/terms/o/operating_expense.asp).
- [37] Zhiyu Jiang. *Installation of offshore wind turbines: A technical review*. Jan. 2021. URL: <https://www.sciencedirect.com/science/article/pii/S1364032120308601>.
- [38] Laura Castro-Santos et al. *Economic feasibility of floating offshore wind farms*. Aug. 2016. URL: <https://www.sciencedirect.com/science/article/pii/S0360544216309094>.



# A

## Appendix A

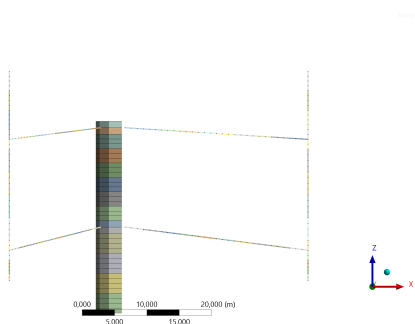


**Figure A.1:** Candidate point 2 from optimization 1 MW fixed, design 1.

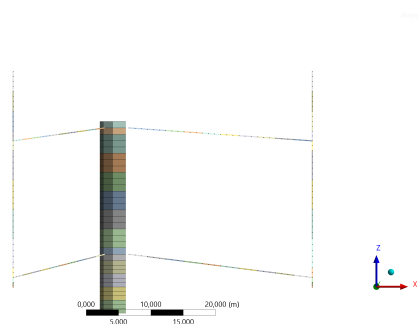


**Figure A.2:** Candidate point 3 from optimization 1 MW fixed, design 1.

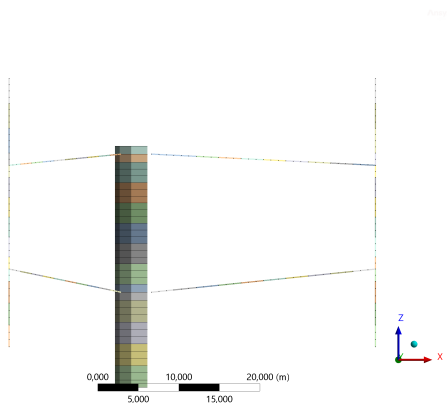


**Figure A.3:** Candidate point 2 from optimization 1 MW pinned, design 1.

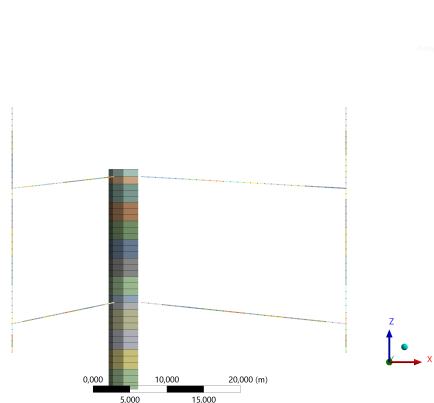


**Figure A.4:** Candidate point 3 from optimization 1 MW pinned, design 1.

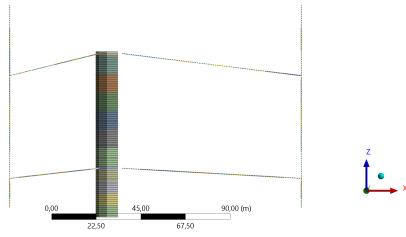


**Figure A.5:** Candidate point 2 from optimization 10 MW fixed, design 1.

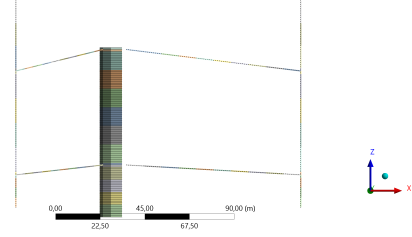


**Figure A.6:** Candidate point 3 from optimization 10 MW fixed, design 1.

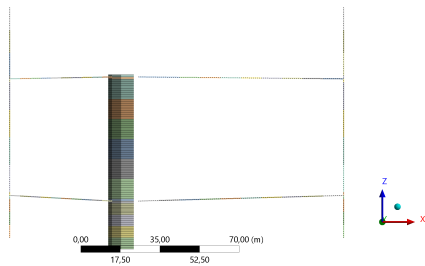


**Figure A.7:** Candidate point 2 from optimization 10 MW fixed, design 2.

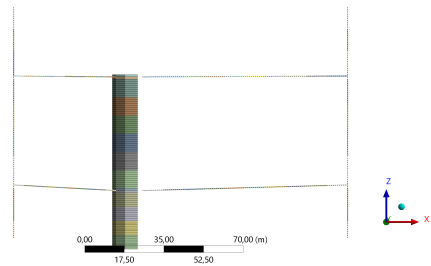


**Figure A.8:** Candidate point 3 from optimization 10 MW fixed, design 2.

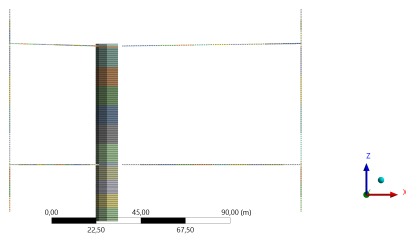


**Figure A.9:** Candidate point 2 from optimization 10 MW pinned, design 1.

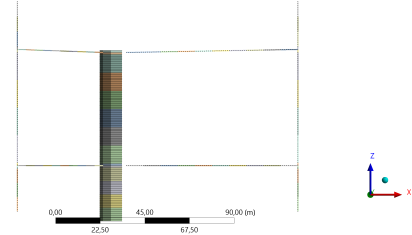


**Figure A.10:** Candidate point 3 from optimization 10 MW pinned, design 1.



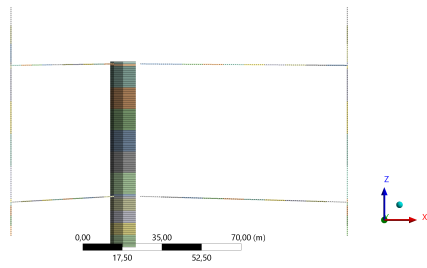


**Figure A.11:** Candidate point 2 from optimization 10 MW pinned, design 2.

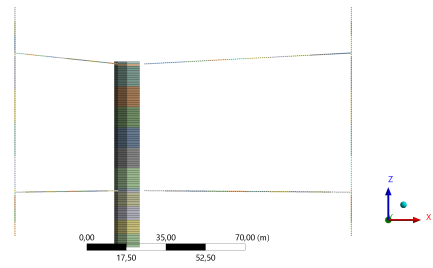


**Figure A.12:** Candidate point 3 from optimization 10 MW pinned, design 2.



# B

## Appendix B

### B.1 1 MW inputs

Name	Value	Name	Value
$VCoG_{\text{rotor}}$	105.1 m	$Cost_{\text{strut}}$	- <sup>2</sup>
$VCoG_{\text{gen.house}}$	90.0 m	$Cost_{\text{blade}}$	- <sup>2</sup>
$VCoG_{\text{spar}}$	21.0 m	$Cost_{\text{tower}}$	- <sup>2</sup>
$m_{\text{strut}}$	15.0 mTon	$Cost_{\text{spar}}$	- <sup>2</sup>
$m_{\text{blade}}$	12.5 mTon	$CoB$	40 m
$m_{\text{tower}}$	94.1 mTon		
$m_{\text{rotor}}$	121.6 mTon		
$m_{\text{gen.house}}$	160.0 mTon		
$m_{\text{spar}}$	929.9 mTon		

**Table B.1:** Inputs for the cost analysis for the 1 and 10 MW cost weight analysis.

$V$ [m/s]	Probability of $V$ [%]	$C_d$ [-]	$A$ [m <sup>2</sup> ]	$\rho_{\text{air}}$ [kg/m <sup>3</sup> ]	$F_{\text{th}}$ [kN]	$L_{\text{blade}}$ [m]	$M_{\text{th}}$ [kNm]
4	30.37	0.775	1993	1.225	15.13	39.85	377
6	22.76	0.759	1993	1.225	33.35	39.85	831
8	17.58	0.774	1993	1.225	60.46	39.85	1507
10	13.38	0.716	1993	1.225	87.39	39.85	2178
12	7.74	0.701	1993	1.225	123.20	39.85	3071
14	4.22	0.575	1993	1.225	137.55	39.85	3429
16	2.27	0.460	1993	1.225	143.72	39.85	3582
18	1.00	0.380	1993	1.225	150.26	39.85	3746
20	0.68	0.327	1993	1.225	159.64	39.85	3979

**Table B.2:** The inputs for the thrust moment calculations for the 1 MW rotors.

---

<sup>2</sup>Confidential data

$R_o$ [m]	$t$ [m]	$R_i$ [m]	$\Delta\sigma$ [MPa]	$n$ [-]	$N$ [-]	Damage [-]
2.0	0.017	1.983	3.58	$1.84 \cdot 10^7$	$6.89 \cdot 10^{12}$	0.0000030
2.0	0.017	1.983	7.88	$2.06 \cdot 10^7$	$1.33 \cdot 10^{11}$	0.000156
2.0	0.017	1.983	14.3	$2.13 \cdot 10^7$	$6.78 \cdot 10^9$	0.00314
2.0	0.017	1.983	20.7	$2.02 \cdot 10^7$	$1.07 \cdot 10^9$	0.0188
2.0	0.017	1.983	29.1	$1.17 \cdot 10^7$	$1.93 \cdot 10^8$	0.0607
2.0	0.017	1.983	32.5	$6.38 \cdot 10^6$	$4.25 \cdot 10^7$	0.150
2.0	0.017	1.983	34.0	$3.46 \cdot 10^6$	$3.72 \cdot 10^7$	0.0930
2.0	0.017	1.983	35.5	$1.56 \cdot 10^6$	$3.26 \cdot 10^7$	0.0480
2.0	0.017	1.983	37.7	$1.06 \cdot 10^6$	$2.72 \cdot 10^7$	0.0392

**Table B.3:** The inputs and results for the S-N curve calculations for the 1 MW models.

Blade	MinTension		MaxTension	
	$F_x$	$F_y$	$F_x$	$F_y$
Blade 1	27	6.4	13	2.9
Blade 2	0.51	0.057	13	1.1
Blade 3	9.5	0.64	2.5	0.38

**Table B.4:** The factors used to scale the forces from the Principia report.

Part	Name	Value
Tower	$R_o$	2 m
Tower	$E_{\text{tower}}$	210 GPa
Tower	$\nu_{\text{tower}}$	0.3
Tower	$\rho_{\text{tower}}$	7850 kg/m <sup>3</sup>
Strut	Tower to strut connection	2.5 m
Strut	$E_{\text{strut}}$	1.0 GPa
Strut	$\nu_{\text{strut}}$	0.3
Strut	$\rho_{\text{strut}}$	19 kg/m <sup>3</sup>
Strut	Initial $A_{\text{cs}}$	5.38 m <sup>2</sup>
Strut	Relation $I_{zz}/A_{\text{cs}}$	0.0771 m <sup>2</sup>
Strut	Relation $I_{yy}/A_{\text{cs}}$	0.5712 m <sup>2</sup>
Strut	Relation $J/A_{\text{cs}}$	0.0852 m <sup>2</sup>
Blade	$E_{\text{blade}}$	1.0 GPa
Blade	$\nu_{\text{blade}}$	0.3
Blade	$\rho_{\text{blade}}$	38 kg/m <sup>3</sup>
Blade	Initial $A_{\text{cs}}$	3.42 m <sup>2</sup>
Blade	Relation $I_{zz}/A_{\text{cs}}$	0.0265 m <sup>2</sup>
Blade	Relation $I_{yy}/A_{\text{cs}}$	0.486 m <sup>2</sup>
Blade	Relation $J/A_{\text{cs}}$	0.0361 m <sup>2</sup>
Full rotor	$P$	1 MPa
Full rotor	$A$	1993 m <sup>2</sup>

**Table B.5:** Fixed parameters for the 1 MW rotors.

Part	Name	Unit	Dependency
Tower	Height	m	$AP_{\text{strut},2,p}$
Tower	$R_i$	m	see Eq. (5.4)
Strut	$AP_{\text{strut},1}$	m	$AP_{\text{strut},1,p}$
Strut	$AP_{\text{strut},2}$	m	$AP_{\text{strut},2,p}$
Strut	Tilt strut 1	°	$I_{\text{strut},1,p}$
Strut	Tilt strut 2	°	$I_{\text{strut},2,p}$
Strut	$A_{\text{cs}}$	m <sup>2</sup>	$CS_{\text{strut},j}$
Strut	$I_{yy}$	m <sup>4</sup>	$CS_{\text{strut},j}$
Strut	$I_{zz}$	m <sup>4</sup>	$CS_{\text{strut},j}$
Strut	$J$	m <sup>4</sup>	$CS_{\text{strut},j}$
Blade	$L_{\text{blade}}$	m	$R$
Blade	$A_{\text{cs}}$	m <sup>2</sup>	$CS_{\text{blade}}$
Blade	$I_{yy}$	m <sup>4</sup>	$CS_{\text{blade}}$
Blade	$I_{zz}$	m <sup>4</sup>	$CS_{\text{blade}}$
Blade	$J$	m <sup>4</sup>	$CS_{\text{blade}}$

**Table B.6:** Parameters governed by design variables for the 1 MW and 10 MW optimization, index  $j$  stands for strut 1 or 2.

## B.2 10 MW inputs

$V$ [m/s]	Probability of $V$ [%]	$C_d$ [-]	$A$ [m <sup>2</sup> ]	$\rho_{\text{air}}$ [kg/m <sup>3</sup> ]	$F_{\text{th}}$ [kN]	$L_{\text{blade}}$ [m]	$M_{\text{th}}$ [kNm]
4	30.37	0.775	19930	1.225	151.3	141.3	11450
6	22.76	0.759	19930	1.225	333.5	141.3	25230
8	17.58	0.774	19930	1.225	604.6	141.3	45740
10	13.38	0.716	19930	1.225	873.9	141.2	66120
12	7.74	0.701	19930	1.225	1232	141.3	93210
14	4.22	0.575	19930	1.225	1375	141.3	104100
16	2.27	0.460	19930	1.225	1437	141.3	108700
18	1.00	0.380	19930	1.225	1503	141.3	113700
20	0.68	0.327	19930	1.225	1596	141.3	120800

**Table B.7:** The inputs for the thrust moment calculations for the 10 MW rotors.

$R_o$ [m]	$t$ [m]	$R_i$ [m]	$\Delta\sigma$ [MPa]	$n$ [-]	$N$ [-]	Damage [-]
5.64	0.051	5.589	4.55	$5.58 \cdot 10^6$	$1.54 \cdot 10^{10}$	0.000361
5.64	0.051	5.589	10.0	$6.27 \cdot 10^6$	$1.44 \cdot 10^9$	0.00435
5.64	0.051	5.589	17.5	$6.46 \cdot 10^6$	$2.73 \cdot 10^8$	0.0237
5.64	0.051	5.589	26.3	$6.14 \cdot 10^6$	$8.02 \cdot 10^7$	0.0766
5.64	0.051	5.589	37.1	$4.27 \cdot 10^6$	$2.86 \cdot 10^7$	0.149
5.64	0.051	5.589	41.4	$2.33 \cdot 10^6$	$2.06 \cdot 10^7$	0.113
5.64	0.051	5.589	43.3	$1.25 \cdot 10^6$	$1.80 \cdot 10^7$	0.0694
5.64	0.051	5.589	45.2	$5.51 \cdot 10^5$	$1.58 \cdot 10^7$	0.0349
5.64	0.051	5.589	48.1	$3.75 \cdot 10^5$	$1.32 \cdot 10^7$	0.0285

**Table B.8:** The inputs and results for the S-N curve calculations for the 10 MW models.

Part	Name	Value
Tower	$R_o$	5.64 m
Tower	$E_{\text{tower}}$	210 GPa
Tower	$\nu_{\text{tower}}$	0.3
Tower	$\rho_{\text{tower}}$	7850 kg/m <sup>3</sup>
Strut	Tower to strut connection	7.83 m
Strut	$E_{\text{strut}}$	1.0 GPa
Strut	$\nu_{\text{strut}}$	0.3
Strut	$\rho_{\text{strut}}$	19 kg/m <sup>3</sup>
Strut	Initial $A_{\text{cs}}$	42.7 m <sup>2</sup>
Strut	Relation $I_{zz}/A_{\text{cs}}$	0.613 m <sup>2</sup>
Strut	Relation $I_{yy}/A_{\text{cs}}$	4.54 m <sup>2</sup>
Strut	Relation $J/A_{\text{cs}}$	0.678 m <sup>2</sup>
Blade	$E_{\text{blade}}$	1.0 GPa
Blade	$\nu_{\text{blade}}$	0.3
Blade	$\rho_{\text{blade}}$	38 kg/m <sup>3</sup>
Blade	Initial $A_{\text{cs}}$	27.2 m <sup>2</sup>
Blade	Relation $I_{zz}/A_{\text{cs}}$	0.211 m <sup>2</sup>
Blade	Relation $I_{yy}/A_{\text{cs}}$	3.87 m <sup>2</sup>
Blade	Relation $J/A_{\text{cs}}$	0.287 m <sup>2</sup>
Full rotor	$P$	10 MPa
Full rotor	$A$	19930 m <sup>2</sup>

**Table B.9:** Fixed parameters for the 10 MW rotors.

DEPARTMENT OF MECHANICS AND MARITIME SCIENCES  
CHALMERS UNIVERSITY OF TECHNOLOGY  
Gothenburg, Sweden  
[www.chalmers.se](http://www.chalmers.se)



**CHALMERS**  
UNIVERSITY OF TECHNOLOGY